

RESEARCH

Open Access



# Involvement of sphingosine-1-phosphate receptor 1 in pain insensitivity in a BTBR mouse model of autism spectrum disorder

Lili Fan<sup>1†</sup>, Qi Li<sup>2†</sup>, Yaxin Shi<sup>1</sup>, Xiang Li<sup>1</sup>, Yutong Liu<sup>1</sup>, Jiaqi Chen<sup>1</sup>, Yaqi Sun<sup>1</sup>, Anjie Chen<sup>1</sup>, Yuan Yang<sup>1</sup>, Xirui Zhang<sup>1</sup>, Jia Wang<sup>1</sup> and Lijie Wu<sup>1,3\*</sup>

## Abstract

**Background** Abnormal sensory perception, particularly pain insensitivity (PAI), is a typical symptom of autism spectrum disorder (ASD). Despite the role of myelin metabolism in the regulation of pain perception, the mechanisms underlying ASD-related PAI remain unclear.

**Methods** The pain-associated gene *sphingosine-1-phosphate receptor 1* (*S1PR1*) was identified in ASD samples through bioinformatics analysis. Its expression in the dorsal root ganglion (DRG) tissues of BTBR ASD model mice was validated using RNA-seq, western blot, RT-qPCR, and immunofluorescence. Pain thresholds were assessed using the von Frey and Hargreaves tests. Patch-clamp techniques measured KCNQ/M channel activity and neuronal action potentials. The expression of *S1PR1*, KCNQ/M, mitogen-activated protein kinase (MAPK), and cyclic AMP/protein kinase A (cAMP/PKA) signaling proteins was analyzed before and after inhibiting the S1P-S1PR1-KCNQ/M pathway via western blot and RT-qPCR.

**Results** Through integrated transcriptomic analysis of ASD samples, we identified the upregulated gene *S1PR1*, which is associated with sphingolipid metabolism and linked to pain perception, and confirmed its role in the BTBR mouse model of ASD. This mechanism involves the regulation of KCNQ/M channels in DRG neurons. The enhanced activity of KCNQ/M channels and the decreased action potentials in small and medium DRG neurons were correlated with PAI in a BTBR mouse model of ASD. Inhibition of the S1P/S1PR1 pathway rescued baseline insensitivity to pain by suppressing KCNQ/M channels in DRG neurons, mediated through the MAPK and cAMP/PKA pathways. Investigating the modulation and underlying mechanisms of the non-opioid pathway involving *S1PR1* will provide new insights into clinical targeted interventions for PAI in ASD.

**Conclusions** *S1PR1* may contribute to PAI in the PNS in ASD. The mechanism involves KCNQ/M channels and the MAPK and cAMP/PKA signaling pathways. Targeting *S1PR1* in the PNS could offer novel therapeutic strategies for the intervention of pain dysesthesias in individuals with ASD.

**Keywords** Pain insensitivity, Autism spectrum disorder, BTBR model mice, Sphingosine-1-phosphate, KCNQ/M potassium channels

<sup>†</sup>Lili Fan and Qi Li contributed equally to this work.

\*Correspondence:

Lijie Wu

hydwlj@ems.hrbmu.edu.cn

Full list of author information is available at the end of the article



## Background

Autism spectrum disorder (ASD) is a serious neurodevelopmental disorder that occurs during early developmental stages. Aberrant sensory perception is recognized as a core diagnostic feature of ASD [1]. In the DSM-5-TR, the American Psychiatric Association has updated the diagnostic criteria for ASD to include hyper- or hyporeactivity to sensory input, with “apparent indifference to pain and temperature” as a symptom of ASD [2]. Extensive sensory abnormalities, such as abnormal auditory sensitivity [3]; smell and taste abnormalities [4]; and disturbances in pain and touch perception [5], are common and significantly impact the quality of life for individuals with ASD [6–8]. Pain insensitivity (PAI) has recently attracted considerable interest. One study reported that 40% of 20–54-month-old children with ASD exhibited altered reactivity to pain [9], while another study indicated that pain perception was reduced by 40% in children with ASD [10]. Recurrent self-injurious behavior and chronic PAI are prevalent in patients with ASD, leading to devastating consequences for their physical and mental health, which has aroused widespread concern [11, 12].

Most studies on ASD pain have focused on molecular genetics [13] and neuroimaging [14]. Individuals with ASD exhibit diminished neural pain responses to sustained pain [15], and abnormalities in the heat-evoked potential pathways of the peripheral nervous system have been demonstrated [16]. Additionally, different ASD mouse models have shown varied behavioral phenotypes related to PAI [17]. Deletion of methyl CpG binding protein 2 (*Mecp2*) or gamma-aminobutyric acid type A receptor subunit beta3 (*Gabrb3*) in the somatosensory neurons of the peripheral nervous system leads to tactile paresthesia and an ASD-like syndrome [18]. In a complete *Shank3* knockdown ASD mouse model, heat pain perception was impaired in both inflammatory and neuropathic models [19]. However, the mechanism by which individuals with ASD experience PAI remains unclear. Several studies have established that lipid metabolism plays a prominent role in the etiology of ASD [13]. Abnormalities in lipid metabolism, particularly in lipoproteins related to social interactions, could also contribute to the pathogenesis of ASD [20]. Our recent serum metabolomics study revealed that elevated sphingosine-1-phosphate (S1P) levels in children with ASD were positively associated with the clinical ASD phenotypes [21]. Furthermore, reducing S1P levels may potentially regulate deficits in social interaction and repetitive behaviors associated with the ASD mouse model [22]. S1P is a sphingolipid metabolite [23], and untargeted metabolomics has revealed a significant link between pain and alterations in sphingolipid metabolism [24]. However, the specific roles and mechanisms of

sphingolipid metabolites in ASD pain perception are still to be elucidated.

The regulation of S1P in pain is independent of endogenous opioid circuits, and S1P along with its receptors are promising therapeutic targets [25]. The excitability of DRG neurons is induced by S1P via activation of S1PR1 and S1PR3 [26]. Mechanoreceptor excitability is regulated by S1PR3 via *KCNQ2/3* channels, while S1P/S1PR3 signaling regulates neuronal excitability and mechanical pain thresholds [27]. *KV7/M* channels, encoded by the *KCNQ* gene family (*KCNQ1–5*), are a subset of voltage-gated  $K^+$  channels that reside on DRG neuron membranes. They exert a significant modulatory effect on neuronal excitability and play a crucial role in pain signaling, especially in the peripheral somatosensory system [28]. Both native and mutant *KV7* channels alter the control of action potentials, which could be a potential causative mechanism of ASD [29]. *KCNQ2/3* potassium channels significantly influence nociceptor neuronal excitability and stabilize membrane potentials [30]. Overall, S1PR1 and *KCNQ/M* channels are closely associated with PAI in ASD. Further studies are required to elucidate the underlying mechanisms.

In this study, we explored the relationship between S1PR1 and PAI in ASD, as identified from a database. This association and its underlying mechanisms were validated using the DRG of *BTBR T+Itpr3tf/J* (*BTBR*) mouse model of ASD. We observed increased S1PR1 expression and activated *KCNQ/M* channels in the DRG neurons of these mice. Inhibition of S1PR1 or *M* channels ameliorates PAI observed in *BTBR* mice. Furthermore, S1PR1 inhibition reduced *KCNQ/M* channels activity, and the *MAPK* and *cAMP/PKA* signaling pathways were involved in this modulation. Additionally, we discovered that S1PR1 levels are regulated by an upstream sphingosine kinase (*SphK*). By targeting S1PR1, we confirmed its role in PAI associated with ASD and elucidated its upstream and downstream mechanisms, suggesting a novel preclinical intervention for ASD patients with PAI.

## Methods

### Animals

*BTBR T+Itpr3tf/J* (*BTBR*) male mice, aged 6–8 weeks, served as the ASD model and were generated at The Jackson Laboratory. *C57BL/6 J* male mice (6–8 weeks) were obtained from Beijing Vital River Laboratory Animal Technology Co., Ltd. To ensure that any observed changes were not influenced by confounding factors, we implemented a standardized controlled environment. Mice were individually housed under a 12-h light/dark cycle, with controlled temperature of  $21 \pm 1$  °C and humidity at  $55 \pm 5\%$ , and were provided food and water ad libitum. All experimental groups and conditions were

blinded to the experimenters to maintain the study's integrity. This controlled environment was established before behavioral testing to allow for acclimatization and to minimize any potential stress or environmental influences on the results.

### Intrathecal injection

The baseline pain response of the mice was assessed the day before intrathecal injection. On the day of the injection, the mice were first left in their cages for 30 min for acclimation. A 25  $\mu$ L Hamilton micro syringe was used for direct transcutaneous intrathecal injection around the lumbar vertebral segments L4/L5 or L5/L6. The experimental group received 10  $\mu$ L of the drugs, while the control group was administered 10  $\mu$ L of the vehicle. The drugs used in this study were as follows: W146 (5  $\mu$ M, 857390P, Sigma-Aldrich, USA), CAY10444 (10  $\mu$ M, 10,005,033, Cayman Chemical, USA), S1P (10  $\mu$ M, 73,914, Sigma-Aldrich, USA), and XE-991 (30  $\mu$ M, X2254, Sigma-Aldrich, USA). Behavioral tests were conducted again 0.5 to 2 h post-injection, according to the experimental needs to assess alterations in pain perception.

### Establishment of chronic pain models

Two chronic pain mice models were used in this study. Deep anesthesia was used in all surgical procedures. A chronic constriction injury (CCI) model was used [31] and adapted for mice [32]. Briefly, mice were immobilized, skin was incised, and the sciatic nerve was exposed. Loose ligation (chromic gut 5.0) was tied to the proximal end of the sciatic nerve until a brief convulsion occurred in the hind limb. The incision was closed with 5–0 nylon sutures. In sham surgeries, the sciatic nerve was exposed without ligation.

Chronic inflammatory pain was induced using complete Freund's adjuvant (CFA) [33], purchased from Sigma (F5881, Sigma-Aldrich, USA). Briefly, a solution (25  $\mu$ L) mixed with phosphate-buffered saline (PBS) at a ratio of 2:1 was injected into the left hind paws of the mice. Control animals received PBS. Subsequently, the animals were sacrificed and the left DRGs (L4-L6) were extracted for further experiments.

### Establishment of acute pain models

Capsaicin (HY-10448, MCE, USA) was injected intraplantarly to induce acute pain in mice. Mice's left hind paws were injected with a solution of capsaicin fully dissolved in DMSO (20  $\mu$ L, 0.5 g/L). Nociceptive intensity was assessed by measuring the total duration of licking behavior within 5 min following capsaicin injection.

### Behavioral testing

Double-blind testing was employed for all behavioral tests, with one experimenter responsible for injecting the mice and the other conducting the behavioral testing. Mice were acclimated for 30 min in cages or on platforms before the behavioral tests.

Two tests were performed to evaluate pain perception. Mechanical hypersensitivity was assessed using the up-down testing method with von Frey filaments (Aesthesio<sup>®</sup>, DanMic Global, LLC, San Jose, CA, USA) [34]. A series of calibrated filaments were applied perpendicularly to the plantar surface of the injected hind paw five times at 10-s intervals. Positive responses to the von Frey test included rapid paw withdrawal, shaking of the affected paw, licking, flinching, or biting. The smallest filament that evoked positive responses in three of the five trials was considered the paw withdrawal threshold.

Hargreaves test system (PL-200, Chengdu Techman Software Co. Ltd., China) was used to assess thermal hypersensitivity. Mice were acclimated to the testing platform for 30 min. Radiant heat at 50% intensity was subsequently applied to the plantar surface of the injected paw. Paw withdrawal latency was measured using sensors that detected positive responses such as flinching, licking, biting, shaking, or rapid withdrawal of the paw. The latency between the onset of heat exposure and paw withdrawal was accurately recorded [35].

### Spinal cord dissections

Mice were anesthetized and sacrificed by decapitation. The L4-L6 spinal column segment and associated tissue were removed, with surrounding skin and muscles carefully trimmed away. Hydraulic extrusion was used to isolate the spinal cord [36], which was then placed in an Eppendorf tube and preserved at  $-80^{\circ}\text{C}$ .

### DRG dissections

Mice were anesthetized and sacrificed by decapitation. The spinal column was isolated, muscles were removed, and the column was bisected sagittally. After removing the spinal cord, the left DRGs (L4-L6) were exposed. Individual DRGs were carefully removed using fine forceps and microdissection scissors after clearing the meninges. The DRGs were then placed in Eppendorf tubes and stored at  $-80^{\circ}\text{C}$ .

### Bioinformatics data acquisition

The GSE113834 and GSE64018 datasets were downloaded from the GEO public repository (<https://www.ncbi.nlm.nih.gov/geo/>). Additionally, RNA-seq analysis was conducted on two other mouse DRG datasets to

extract gene expression matrix data for subsequent analysis. This study included all available samples. The datasets are listed in Additional file 1: Table S1.

### Identification of ASD differentially expressed genes (DEGs) and key co-expression modules

We employed weighted gene co-expression network analysis (WGCNA) to identify DEGs and key co-expression modules associated with ASD. WGCNA constructs co-expression networks by clustering genes with similar expression patterns and evaluating their correlations with specific traits or phenotypes. This approach is valuable for identifying candidate genes and biomarkers. Gene expression data from the GSE113834 and GSE64018 datasets were analyzed using the WGCNA R package [37], available on the Comprehensive R Archive Network. The analysis for the GSE113834 dataset was performed with a soft threshold power of 14, and modules were required to have a minimum size of 50 genes. For the GSE64018 dataset, the soft threshold power was set to 13, with the same module size requirement.

The GSE113834 and GSE64018 datasets were analyzed for differential gene expression using the R package limma, with DEGs identified based on a  $p$  value of 0.05. Volcano plots were generated using the ggplot2 package in R to visualize the results. To identify key genes associated with ASD, a Venn analysis was performed on the DEGs and the WGCNA key gene modules from both datasets using the online tool Draw Venn Diagram (<http://bioinformatics.psb.ugent.be/webtools/Venn>). To explore potential interactions among the intersection genes, the STRING database (<https://string-db.org/>) was used to construct a protein–protein interaction (PPI) network, with a confidence score threshold of  $\geq 0.15$ . The results were exported from STRING and visualized for further analysis.

Pain-related gene sets (GOBP\_BEHAVIORAL\_RESPONSE\_TO\_PAIN) were downloaded from the MSigDB database (<https://www.gsea-msigdb.org/gsea/msigdb/>) and analyzed using the R package GSVA to determine their GSVA scores in the GSE64018 dataset. *SIPR1* expression data were extracted from the same dataset. The correlation between the pain gene set and *SIPR1* expression was then analyzed using Pearson's correlation coefficient, with visualization performed using the R packages ggplot2 and gpubr, to explore the relationship between *SIPR1* and pain.

### RNA-seq data verification

In addition, we performed differential analysis using RNA data from mouse L4-6 DRG to explore *SIPR1* expression (detailed data are presented in Additional file 1: Table S1). For the analysis, we used the R package DESeq2. DEGs

were screened using  $p < 0.05$ . Volcano plots were generated using the ggplot2 R package to visualize the results.

### Western blotting analysis

The spinal cord and DRG were mechanically homogenized in RIPA lysis buffer at 4 °C. Lysates were centrifuged at 12,000  $\times g$  for 15 min at 4 °C. Protein quantification was determined using the BCA Protein Assay Kit. For SDS-PAGE, 10% gels were run at constant voltages of 80 and 120 V for the stacking and separating gels, respectively. After electrophoresis, proteins were transferred to a PVDF membrane by electro-transfer at a constant voltage of 68 V. Immunodetection was performed using enhanced chemiluminescence following incubation with primary and secondary antibodies. Densitometry was used to quantify protein expression levels. The monoclonal antibodies used for western blotting were as follows: anti-S1PR1 (Rabbit, 1:1000, 55,133–1-Ap, Proteintech, USA); anti-S1PR3 (Rabbit, 1:1000; NBP2-24,762, Novus, USA); anti-KCNQ2 (Guinea pig, 1:200; AGP-065, Alomone, Israel); anti-KCNQ3 (Rabbit, 1:200; APC-051, Alomone, Israel); anti-KCNQ5 (Rabbit, 1:1000; YT2460, Proteintech, USA); anti-phospho-p44/42 MAPK (Rabbit, 1:2000; 7370S, CST, USA); anti-p44/42 MAPK (Erk1/2) (Rabbit, 1:2000; 4695, CST, USA); anti-phospho-p38 MAPK (Rabbit, 1:1000; 4511S, CST, USA); anti-p38 MAPK (Rabbit, 1:1000; 8690S, CST, USA); anti-PKA (Rabbit, 1:1000; 4782S, CST, USA); anti-phospho-PKA C (Rabbit, 1:1000; 5561S, CST, USA); anti-PKC (Rabbit, 1:1000; ab181558, Abcam, UK); anti-phospho-PKC (Rabbit, 1:1000; 38938S, CST, USA); anti-GADPH (Rabbit, 1:1000; 5174S, CST, USA); anti- $\beta$ -tubulin (Rabbit, 1:2000; 10,094–1-AP, Proteintech, USA); and anti- $\beta$ -actin (Rabbit, 1:1000, 4970 s, CST, USA). Bio-Rad Image Lab software was used for protein quantification.

### RT-qPCR

DRG tissues were dissected and stored at  $-80$  °C until RNA extraction was performed using the TRIzol reagent (15,596,026, Thermo Fisher Scientific, Germany). Subsequently, 1  $\mu g$  of total RNA was reverse-transcribed using the PrimeScript RT Reagent Kit (Takara Bio, Dalian, China). mRNA transcripts were quantified using TB Green™ Premix Ex Taq™ II (Takara Bio, Dalian, China), and real-time qPCR was performed on the Roche Universal Probe Library System [38]. Relative amounts of amplified cDNAs were calculated using on the delta CT method, with each gene assessed in at least three independent experiments. Sequences of PCR primer sets used in this study are listed in Supplementary Additional file 1: Table S2.

### Immunofluorescence

After anesthesia, the mice were transcardially perfused with 50 mL of 0.9% cold saline followed by 50 mL of 4% paraformaldehyde (PFA) over 5 min. The left L4-L6 DRGs were then removed and fixed in 4% PFA for 24 h at 4 °C. Subsequently, the tissues were dehydrated in 10%, 20%, and 30% sucrose solution at 4 °C for 24 h each, before being sectioned at 4 μm using a Leica CM1950 cryostat (Leica Buffalo Grove, USA).

At room temperature, the sections were permeabilized in PBS containing 0.3% TritonX-100 and 5% goat serum for 1 h. Blocking was performed overnight at 4 °C with 5% normal goat serum diluted in PBS. They were then incubated overnight at 4 °C with a mixture of primary antibodies [39]. After three 10-min washes in PBS, a blocking buffer containing secondary antibodies was added, and the sections were incubated for 1.5 h at room temperature, followed by three 10-min washes in PBS. After counterstaining with 4',6-diamidino-2-phenylindole (DAPI) (1:500 dilution, Sigma-Aldrich, Germany) for 5 min, the sections were sealed with an antifluorescence mounting medium. Images were captured under a confocal microscope (LSM780; Zeiss, Germany) using consistent exposure times, offsets, and gains for each staining marker. The monoclonal antibodies used for immunofluorescence were as follows: anti-S1PR1 (Rabbit, 1:250; ab7707b, Abcam, UK); anti-KCNQ2 (Guinea pig, 1:200; AGP-065, Alomone, Israel); and anti-KCNQ5 (Rabbit, 1:200; APC-155, Alomone, Israel). ImageJ software (NIH, Bethesda, MD, USA) was used to analyze the mean immunoreactive density in the DRG [40]. All quantification procedures were blinded to animal groups and treatments.

### Culture of DRG neurons

For whole-cell patch-clamp recordings, L4-L6 DRG neurons were isolated from mice and cultured. The ganglia were removed and placed in ice-cold Hanks' balanced salt solution (HBSS). They were then digested in a solution containing Collagenase Type 2 (2 mg/mL, LS004176, Worthington, USA) and Dispase II protease (7.5 mg/mL, D4693-1G, Sigma-Aldrich, USA) for 35 min in a 5% CO<sub>2</sub> incubator at 37 °C. The digestion was terminated using Dulbecco's Modified Eagle Medium (DMEM) supplemented with 10% fetal bovine serum (ThermoFisherScientific, USA). The isolated cells were collected by centrifugation at 12,000×g for 5 min and suspended in 10% DMEM. The cells were then placed on a poly d-lysine-coated glass coverslips and allowed to adhere for 3–4 h. Following adhesion, an appropriate volume of 10% DMEM was added for continued culture. Until experiments were conducted, the

cells were maintained in a humidified atmosphere of 95% air and 5% CO<sub>2</sub> at 37 °C for 24 h.

### Electrophysiological recordings in dissociated mouse DRG neurons

Whole-cell voltage- and current-clamp recordings were performed on cultured DRG neuron culture at room temperature (23 ± 2 °C). Data were low-pass filtered at 2 kHz and sampled at 5 kHz using an Axopatch-200B amplifier, Axon Digidata 1550 B, and pClamp software. Recording electrodes had a resistance of 2–5 MΩ. For action potential recordings, the internal solution contained (in mM): 140 KCl, 4 NaCl, 10 HEPES, 10 EGTA, 0.5 CaCl<sub>2</sub>, and 1 MgCl<sub>2</sub>; the pH was adjusted to pH 7.2 with KOH. The bath solution contained (in mM): 140 NaCl, 5 KCl, 1.8 CaCl<sub>2</sub>, 1 MgCl<sub>2</sub>, 10 HEPES, and 10 glucose; the pH was adjusted to pH 7.4 with NaOH, and the osmolarity was set to 320 Osm with sucrose. Action potentials were induced using a series of stepwise stimulations.

For M-current recordings, the internal solution contained (in mM): 80 K acetate, 30 KCl, 40 HEPES, 3 MgCl<sub>2</sub>, 3 EGTA, and 1 CaCl<sub>2</sub>; the pH was adjusted to 7.2 with KOH. The bath solution contained (in mM): 144 NaCl, 2.5 KCl, 2 CaCl<sub>2</sub>, 0.5 MgCl<sub>2</sub>, 5 HEPES, and 10 glucose; the pH was adjusted to pH 7.4 with NaOH. In the current-clamp experiments, the M-current was activated by 1-s hyperpolarizing pulses from –20 to –60 mV, and the M-current tail was observed at –60 mV. The current density (pA/pF) was determined by normalizing the current amplitude to the membrane capacitance [27]. Amphotericin B (1 mg) was then dissolved in 20 μL DMSO as a stock solution and protected from light until use. A 2 μL aliquot of the stock solution was mixed with 1 mL of the internal solution and used within 2 h.

### Statistical analysis

Statistical analyses were conducted using SPSS 26. Data are reported as the mean ± SEM, with a significance threshold of  $\alpha=0.05$  (n.s.  $p>0.05$ , \* $p<0.05$ , \*\* $p<0.01$ , \*\*\* $p<0.001$ , \*\*\*\* $p<0.0001$ ). The Shapiro–Wilk test was used to assess the normality of the data distribution. Student's *t*-test was used to compare two groups, and one-way analysis of variance (ANOVA) was used to compare three groups. Welch's correction was applied if the assumption of variance homogeneity was violated. The Kruskal–Wallis test was used for comparisons between groups when normality or normality criteria were violated.

## Results

### Discovering and verifying the mechanisms of S1PR1 signaling in ASD PAI

The experimental design of this study is illustrated in Fig. 1. We first identified *S1PR1* as a candidate gene in

patients with ASD using the GEO database. Correlation analysis revealed a moderate association between *S1PR1* expression and pain, highlighting *S1PR1* as a differentially expressed gene of interest. Subsequently, we observed impaired baseline mechanical pain in BTBR mice, which could be ameliorated by inhibiting *S1PR1*. Additionally, elevated *S1PR1* expression was detected in pain-sensing small to medium diameter DRG neurons in these mice. To explore the underlying mechanisms, we conducted electrophysiological experiments on DRG neurons, confirming the suppression of evoked action potentials and activation of KCNQ/M potassium channels in small to medium diameter DRG neurons of BTBR mice. Furthermore, we discovered that the overexpression of *S1PR1* in ASD is modulated by SphK, and that the inhibition of *S1PR1* downregulated activated KCNQ/M potassium channels in DRG neurons, thereby improving baseline PAI. The MAPK and cAMP/PKA pathways are also involved in this process. Targeting the SphK/*S1P*/*S1PR1* signaling pathway might present a potential novel therapeutic approach for PAI in patients with ASD.

**S1PR1 as a potential molecular target in ASD**

To identify the genes most associated with ASD, WGCNA was constructed using the GSE113834 (Dataset

1) and GSE64018 (Dataset 2) datasets with the WGCNA R package (Fig. 2a and b). Seven modules were identified in Dataset 1 (Fig. 2c) and nine in Dataset 2 (Fig. 2d). These modules are represented in heatmaps illustrating module-trait relationships, showing the correlation of each module with ASD traits. In WGCNA, modules represent clusters of genes with similar expression patterns, and those with the highest correlation to a specific phenotype are typically selected for further investigation [41, 42]. Accordingly, the brown module from Dataset 1 and the turquoise module from Dataset 2 were of particular interest due to their strong correlations with ASD traits. These modules were selected for subsequent analysis, as they may identify candidate genes and biomarkers relevant to ASD. Our analysis suggests that these modules are enriched in genes that may play pivotal roles in ASD pathophysiology, as evidenced by their pronounced correlation with ASD phenotypes. We identified 2526 differentially expressed genes (DEGs) from Dataset 1 (Fig. 2e), including 1084 upregulated and 1442 downregulated genes. In Dataset 2, 5704 DEGs were identified (Fig. 2f), consisting of 2695 upregulated and 3009 downregulated genes. Notably, *S1PR1* was upregulated in both datasets.

Using Venn analysis, we analyzed the DEGs with the most prominent brown and turquoise modules in the

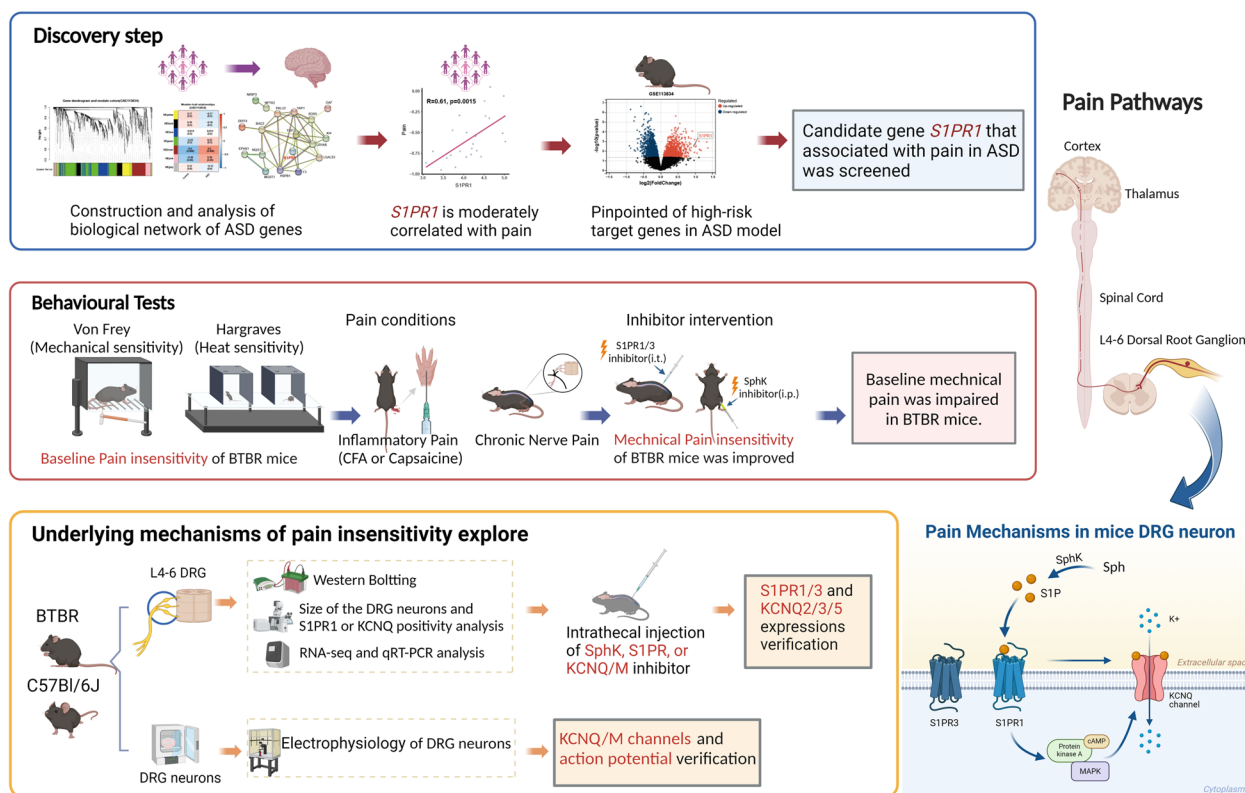


**Fig. 1** Overall workflow diagram for discovering and verifying the roles and mechanisms of PAI in ASD

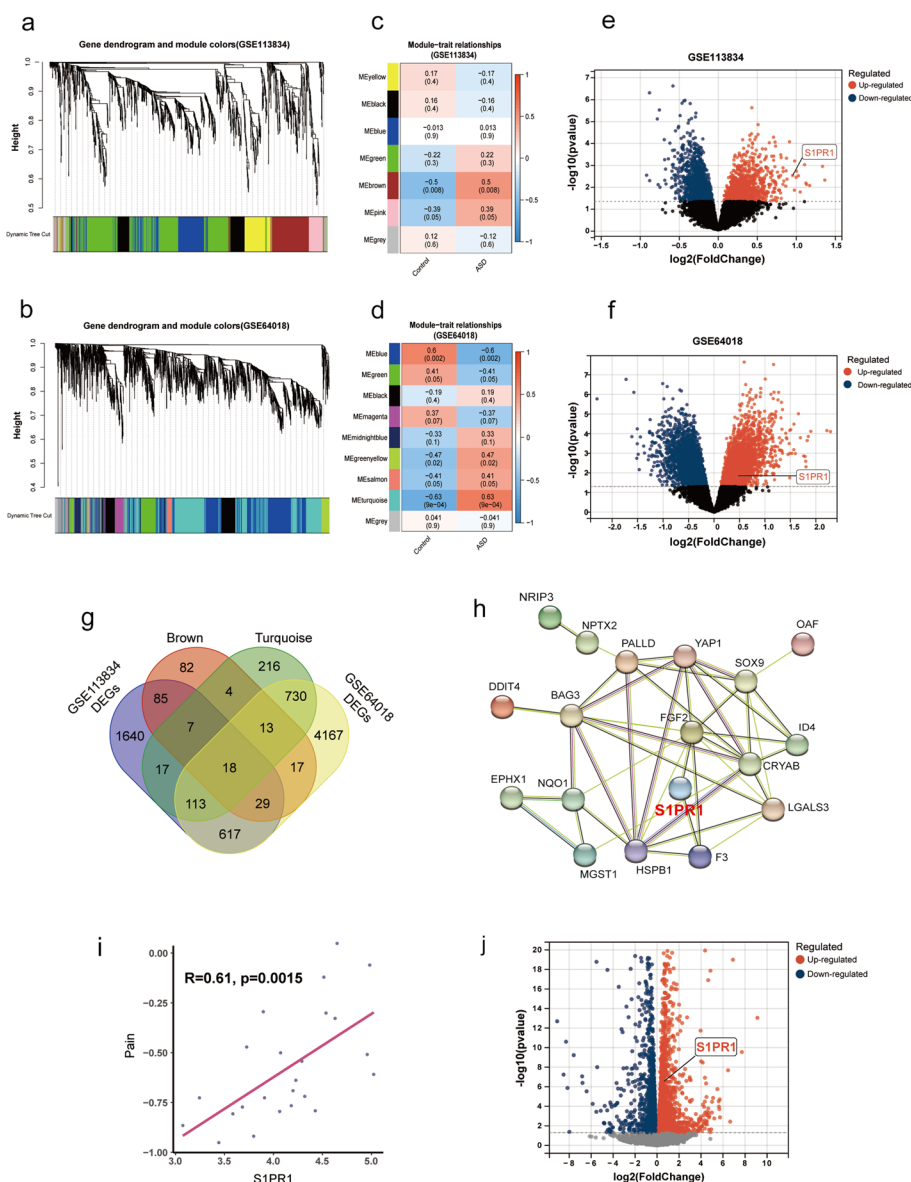


**Fig. 2** Identification of key gene modules from the GSE113834 and GSE64018 datasets via WGCNA. **a** and **b** Clustering tree diagram of the co-expression network module. The bottom of the graph represents different colored clustering gene modules. **c** and **d** Heatmap showing module-trait relationships. The cells represent the correlation and *p* value of the corresponding color module in the Con or ASD group. The redder the cell color, the stronger the positive correlation, and the bluer the stronger the negative correlation. **e** and **f** Volcano plot of DEGs. Red represents upregulated genes, and blue represents downregulated genes. **g** Identification of 18 common DEGs. WGCNA key gene modules from the GSE113834 and GSE64018 datasets. **h** PPI network of 18 genes. It consists of 18 nodes and 44 edges. **i** Correlation analysis between *S1PR1* and pain. **j** Volcano plot showing the DEGs from the RNA-seq mice data 1 (Additional file 1: Table S1). The red color represents upregulated genes, and the blue color represents downregulated genes

WGCNA of the two datasets and identified 18 common genes that are likely important in ASD (Fig. 2g), including *SP1R1*, *SOX9*, *LGALS3*, *CRYAB*, *DDIT4*, *ID4*, *NQO1*, *FGF2*, *NRIP3*, *F3*, *HSPB1*, *PALLD*, *MGST1*, *BAG3*, *NPTX2*, *EPHX1*, *OAF*, and *YAP1*, suggesting the involvement of *S1PR1* in ASD pathophysiology. To investigate potential interactions among these 18 genes, a PPI

network was constructed using the STRING database, including 18 nodes and 44 edges (Fig. 2h). Genes that are closely connected to network nodes typically have significant biological functions and are closely related to other nodes within the network.

A correlation analysis was performed between the expression levels of *S1PR1* in Dataset 2 and the GSEA

scores of the pain gene set. The results demonstrated statistical significance, with a  $p$  value of less than 0.05. Additionally, a moderate correlation ( $R=0.61$ ) was observed between *SIPR1* and ASD pain (Fig. 2i).

DRG are the initial sensory relay for pain perception and play a crucial role in processing nociceptive signals [43]. To further explore *SIPR1* expression in the ASD BTBR mouse model, differential analysis of DRG RNA-seq data 1 (Additional file 1: Table S1) was performed. We identified 4453 DEGs, including 2305 upregulated and 2148 downregulated genes (Fig. 2j). Compared to control (Con) mice, *SIPR1* expression was significantly higher in BTBR mice. These findings suggest that *SIPR1* is associated with PAI in BTBR mice.

### Baseline pain and inflammatory pain are impaired in the BTBR mice

To investigate the mechanisms of pain regulation in ASD, we first assessed the baseline thermal and mechanical sensitivities in BTBR and Con mice. BTBR mice displayed a significant mechanical insensitivity (Student's  $t$ -test;  $p < 0.0001$ ; Fig. 3a), as evidenced by higher paw withdrawal thresholds to mechanical stimuli in the von Frey test, with mean thresholds of 1.50 g in BTBR mice compared to 0.66 g in Con mice. The term "withdrawal threshold" refers to the minimum noxious stimulus intensity that triggers a withdrawal response, serving as a measure of pain perception. Similarly, the Hargreaves test revealed prolonged withdrawal latencies in response to radiant heat in BTBR mice (Student's  $t$ -test;  $p < 0.0001$ ; Fig. 3b).

Subsequently, we compared multiple nociceptive sensitivities in BTBR and Con mice, including CFA-induced

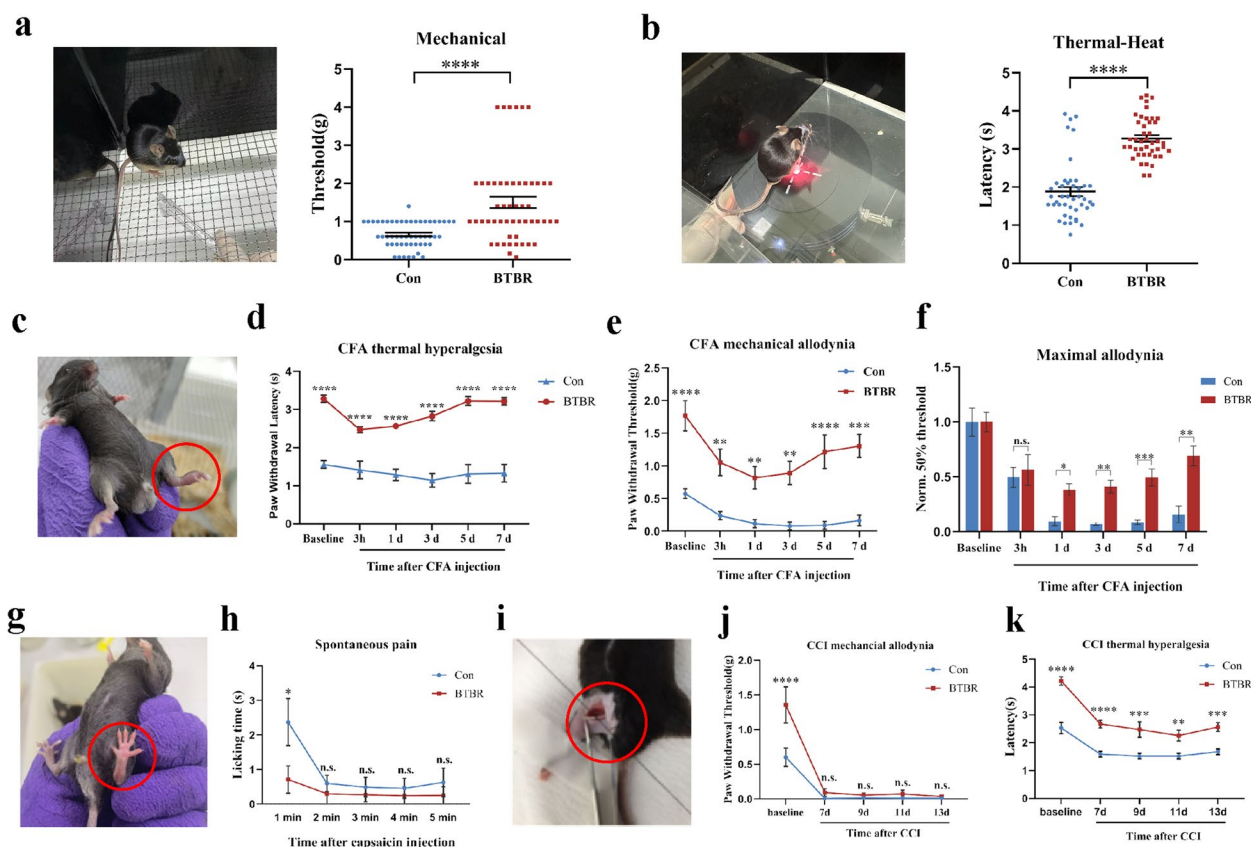


**Fig. 3** BTBR mice exhibit reductions in baseline and inflammation-induced pain. **a** Von Frey test results for baseline mechanical sensitivity.  $n=52$  mice per group. **b** Hargreaves test for baseline heat sensitivity.  $n=43$  mice per group. **c** Alteration in the left hind paw on day 5 after CFA injection in mice. **d** Heat sensitivity after CFA injection in mice.  $n=26$  mice per group. **e** Mechanical sensitivity after CFA injection in mice.  $n=26$  mice per group. **f** Allodynia when von Frey thresholds are normalized to baseline thresholds for each mouse.  $n=26$  mice per group. **g** Alteration in the left hind paw after capsaicin injection. **h** Time course of capsaicin-induced spontaneous pain.  $n=10$  mice per group. **i** Alteration in the left hind paw after CCI. **j** Mechanical sensitivity after CCI.  $n=10$  mice per group. **k** Thermal sensitivity after CCI.  $n=10$  mice per group. All data are shown as bar diagrams, which reflect the arithmetic mean  $\pm$  standard error of the mean. \*  $p < 0.05$ , \*\*  $p < 0.01$ , \*\*\*  $p < 0.001$ , \*\*\*\*  $p < 0.0001$ , n.s. not significantly different

chronic inflammatory pain [1–3] on days 1, 3, 5, and 7; the CCI model of neuropathic pain on days 7, 9, 11, and 13; and capsaicin-induced acute inflammatory pain within 5 min. After the intraplantar injection of CFA, persistent inflammatory pain was induced, and the thermal pain threshold in the BTBR group was significantly higher than that in the Con group (two-way ANOVA;  $p < 0.0001$ ; Fig. 3d). Raghavendra et al. found that CFA-induced peripheral inflammation can lead to central sensitization, which seems to be linked to the influx of various immune cells during the inflammatory process. Both innate and adaptive immune cells are involved [44], and they may affect neurons by releasing cytokines and chemokines, thereby playing a role in pain regulation [45, 46]. Under the combined influence of these mechanisms, there is a decrease in withdrawal response followed by a return to baseline levels. BTBR mice also showed impaired mechanical sensitivity compared to the Con group after the induction of inflammatory pain (two-way ANOVA;  $p < 0.0001$ ; Fig. 3e). Remarkably, BTBR mice exhibited faster recovery in withdrawal threshold following inflammatory pain, with a significant difference observed in maximal allodynia between the BTBR and Con group, particularly on day 5 post-CFA injection (two-way ANOVA;  $p = 0.0005$ ; Fig. 3f). In the capsaicin-induced acute neurogenic inflammation model (paw edema), BTBR mice exhibited reduced spontaneous pain behavior (licking and flinching) 1 min after capsaicin injection compared to Con mice (two-way ANOVA;  $p = 0.01$ ; Fig. 3h). Chronic constriction injuries produced long-lasting neuropathic pain, and although BTBR mice exhibited significant hypersensitivity to neuropathic pain (two-way ANOVA;  $p < 0.0001$ ; Fig. 3j), however, no significant differences were observed compared to the Con group. A significant elevation in the thermal threshold was observed in BTBR mice compared to the Con group (two-way ANOVA;  $p = 0.001$ ; Fig. 3k).

The duration of capsaicin-induced acute pain was transient, whereas BTBR mice exhibited the most significant difference in mechanical pain on day 5 following CFA-induced persistent inflammatory pain. Consequently, CFA-induced persistent inflammatory pain (5 days) was

selected for subsequent studies to investigate the modulation of chronic inflammatory pain in ASD. In summary, these data suggest that BTBR mice have impaired baseline mechanical pain and inflammatory pain.

#### S1PR1 expression was upregulated in the DRGs of BTBR mice

As previously mentioned, S1PR1 is likely implicated in PAI associated with ASD. To further investigate, we validated the expression of pain-associated S1PR1 and S1PR3 in the DRGs and spinal cord tissues. Figure 4a shows that the S1PR1 protein levels (Student's  $t$ -test;  $p = 0.9324$ ) and S1PR3 protein levels (Student's  $t$ -test;  $p = 0.4194$ ) did not significantly differ in the spinal cord tissue between the BTBR and Con group. In contrast, S1PR1 protein expression in the DRGs was significantly upregulated in the BTBR group compared to the Con group (Student's  $t$ -test;  $p = 0.0008$ ; Fig. 4b), which was further confirmed by RT-qPCR analysis (Student's  $t$ -test;  $p = 0.0127$ ; Fig. 4c). However, no significant difference in S1PR3 protein level (Student's  $t$ -test;  $p = 0.1388$ ) was observed between the DRGs of the BTBR and Con group. Quantitative analysis of S1PR1 immunostaining revealed the expression of S1PR1<sup>+</sup> neurons in the BTBR mice. Immunofluorescence results indicated that S1PR1 was widely expressed in DRG neurons (Fig. 4e and f). Specifically,  $44.10 \pm 2.798\%$  of neurons in the Con group expressed S1PR1, whereas the percentage in BTBR neurons was significantly higher at  $56.18 \pm 4.075\%$  (Student's  $t$ -test;  $p = 0.0226$ ). Analysis of cell size distribution showed that S1PR1<sup>+</sup> neurons were widely distributed among DRG neurons of varying sizes, with most being small or medium diameter neurons (Fig. 4g), which play a key role in pain processing [47]. The BTBR group showed higher S1PR1 expression in DRG neurons than the Con group (Student's  $t$ -test;  $p = 0.0226$ ; Fig. 4h). We then assessed alterations in S1PR1 protein levels in DRGs after CFA-induced inflammation. S1PR1 protein expression increased in the BTBR group on CFA day 5 (Kruskal–Wallis test;  $p = 0.0017$ ; Fig. 4i), similar to that observed in the Con group on CFA day 5 (Kruskal–Wallis test;  $p = 0.0033$ ; Fig. 4i). Nevertheless, there was no significant difference in S1PR1

(See figure on next page.)

**Fig. 4** Characterization of S1PR1 and S1PR3 expression in mouse DRGs and spinal cord. **a** Representative western blotting results and quantification of the S1PR1 and S1PR3 protein in mouse spinal cord.  $n = 4$  mice per group. **b** Representative western blotting results and quantification of the S1PR1 and S1PR3 protein in mouse DRGs;  $n = 7–9$  mice per group. **c** Quantification of S1PR1 and S1PR3 mRNA expression in mouse DRGs;  $n = 7–10$  mice per group. **d** Representative fluorescent images of S1PR1 (green) and nuclei (DAPI, blue) in DRG sections of Con and BTBR mice. Scale bars = 100  $\mu\text{m}$ . **e** and **f** Distribution of S1PR1<sup>+</sup> in neurons of different diameters in Con and BTBR mouse DRGs.  $n = 6$  mice per group. **g** Comparison of the percentage of S1PR1<sup>+</sup> neurons in the BTBR and Con group;  $n = 6$  mice per group. **h** Total percentage of S1PR1<sup>+</sup> neurons in the BTBR and Con group.  $n = 10–11$  mice per group. **i** Representative western blotting results and quantification of the S1PR1 protein in mouse DRGs on day 5 after CFA injection in the left paw;  $n = 8$  mice per group. All data are shown as bar diagrams, which reflect the arithmetic mean  $\pm$  standard error of the mean. \*  $p < 0.05$ , \*\*  $p < 0.01$ , \*\*\*  $p < 0.001$ , n.s. not significantly different

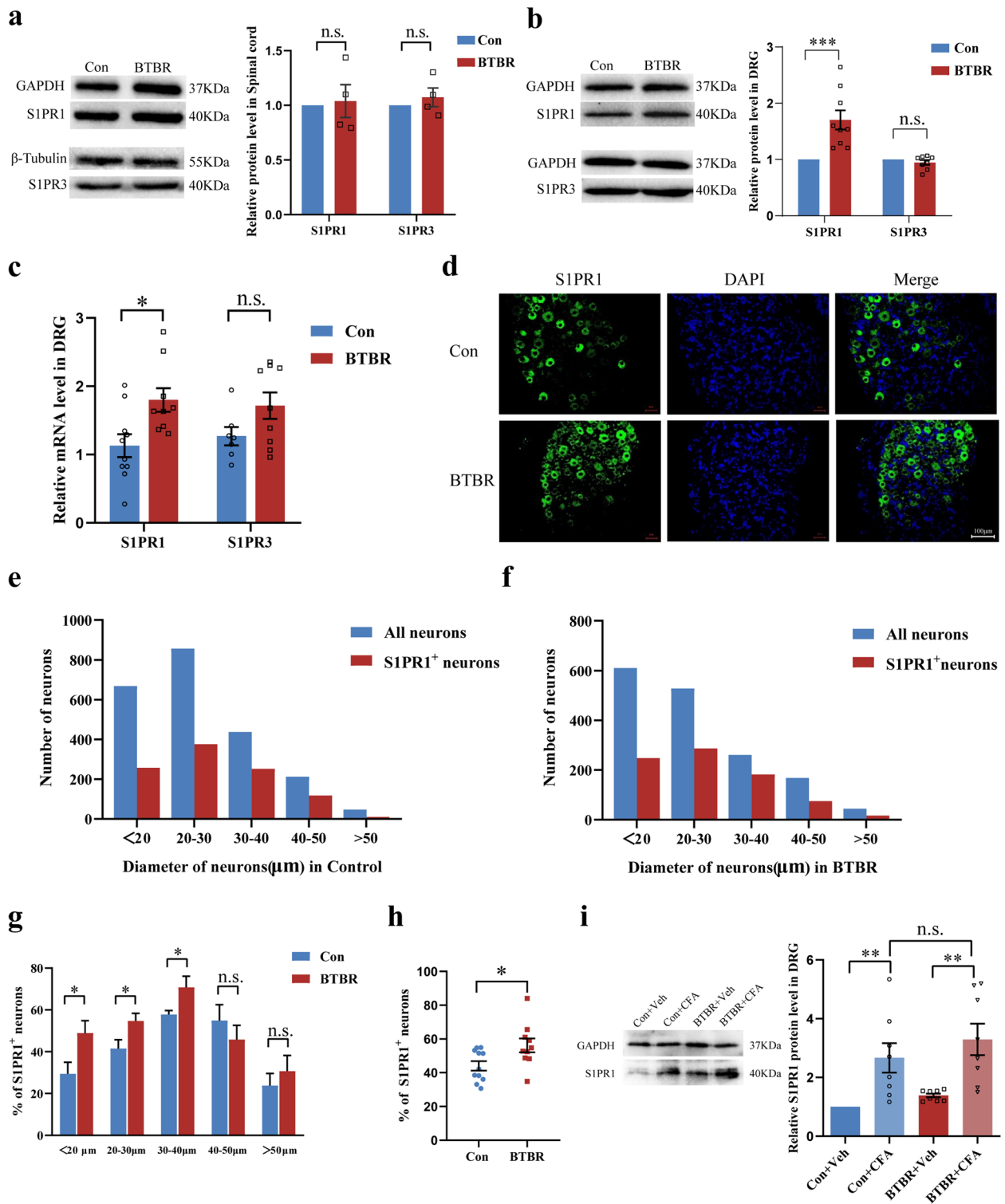


**Fig. 4** (See legend on previous page.)

expression between the BTBR and Con group on CFA day 5 (Kruskal–Wallis test;  $p > 0.9999$ ; Fig. 4i). These results suggest that S1PR1 is involved in the normal development of inflammatory pain in the DRGs of BTBR

mice. Collectively, these findings indicate that baseline PAI in BTBR mice is correlated with the upregulation of S1PR1 in small and medium diameter DRG neurons.

### S1PR1 inhibition rescued PAI in BTBR mice

Considering the elevated S1PR1 levels in the DRGs of BTBR mice, we investigated whether S1PR signaling modulates pain in ASD. BTBR mice were injected intrathecally with either 5  $\mu$ M of the S1PR1 inhibitor W146 or 10  $\mu$ M of the S1PR3 inhibitor CAY10444 (CAY). Results showed that 1 h after W146 administration, the baseline mechanical pain threshold in BTBR mice significantly decreased from  $1.48 \pm 0.13$  to  $0.52 \pm 0.12$  g (Mann–Whitney test;  $p < 0.0001$ ; Fig. 5a). In contrast, the S1PR3 inhibitor CAY10444 had no significant effect on the pain threshold 1 h post-injection (Mann–Whitney test;  $p = 0.2421$ ; Fig. 5b). We assessed the effects of S1PR1 or S1PR3 inhibition on CFA-induced inflammatory hypersensitivity on day 5. The results indicated that inflammatory PAI was rescued in the BTBR+CFA group 1 h after W146 intervention (Mann–Whitney test;  $p = 0.0056$ ; Fig. 5c). However, no significant change was observed after CAY intervention (Mann–Whitney test;  $p = 0.3942$ ; Fig. 5d). These findings suggest that S1PR1 inhibition can ameliorate insensitivity to both baseline and inflammatory pain.

To further investigate, mechanical thresholds were normalized in BTBR and BTBR+CFA mice following W146 intervention to account for baseline pain threshold differences. No significant difference was observed in the normalized pain threshold between the BTBR and BTBR+CFA group after W146 intervention (Student's  $t$ -test;  $p = 0.9188$ ; Fig. 5e). These findings suggest that the increased S1PR1-mediated baseline PAI and inflammatory pain deficits are likely rooted in baseline PAI. Further studies on the role of S1PR1 signaling in PAI in patients with ASD could provide valuable insights.

### M-channel activation inhibited action potentials in BTBR mice DRG neuron-regulated PAI

In DRGs, small-diameter neurons are the primary mediators of pain [47]. These neurons possess M channels that are essential for maintaining neuronal the resting membrane potential [27]; therefore, DRG neurons with diameters of less than 30  $\mu$ m were selected for subsequent electrophysiological experiments. Whole-cell current-clamp and voltage-clamp recordings were conducted to investigate the characteristics of M channels. M-currents were activated by depolarizing the membrane to  $-20$  mV and then hyperpolarizing to  $-60$  mV. The results showed that the slow, voltage-dependent tail current amplitudes were significantly increased in the BTBR group compared to the Con group ( $7.54 \pm 0.35$  pA/pF Con vs.  $11.68 \pm 1.71$  pA/pF BTBR; one-way ANOVA;  $p = 0.0217$ ; Fig. 5g and h). Application of the M channel inhibitor XE-991 (5  $\mu$ M) decreased M-currents in the BTBR+XE-991 group ( $5.01 \pm 0.42$  pA/pF in BTBR+XE-991; one-way ANOVA;

$p = 0.0007$ ; Fig. 5g and h). Moreover, the resting membrane potential (RMP) in the BTBR group was less excitable than in the Con group ( $-56.35 \pm 0.9131$  mV BTBR vs.  $-51.4 \pm 1.326$  mV Con; two-way ANOVA;  $p = 0.0273$ ; Fig. 5i and j). Administration of the M channel inhibitor XE-991 increased the RMP in the BTBR+XE-991 group ( $-51.28 \pm 1.540$  mV in BTBR+XE-991; two-way ANOVA;  $p = 0.0039$ , Fig. 5i and j). Current step injections revealed that BTBR neurons fired fewer action potentials than Con neurons ( $4 \pm 0.6325$  Hz BTBR vs.  $10 \pm 1.452$  Hz Con; two-way ANOVA;  $p = 0.0003$ ; 150 pA, Fig. 5k). However, after administration of XE-991, the action potential frequency in BTBR neurons increased significantly, indicating increased excitability ( $20 \pm 2.828$  Hz in BTBR+XE-991; two-way ANOVA,  $p < 0.0001$ ; 150 pA, Fig. 5k). These findings suggest that the increased activation of M channels in DRG neurons contributes to PAI in BTBR mice.

The expression of KCNQ2, KCNQ5, and KCNQ3, which constitute the M channels in DRG neurons of Con and BTBR mice, were assessed using molecular biological techniques. BTBR mice exhibited higher RNA levels of KCNQ2 (Student's  $t$ -test;  $p = 0.0226$ ; Fig. 6a) and KCNQ5 (Student's  $t$ -test;  $p = 0.0013$ ; Fig. 6b) compared to Con mice. In contrast, KCNQ3 expression showed no significant difference (Student's  $t$ -test;  $p = 0.3995$ ; Fig. 6c). These findings were corroborated by western blot analysis, which confirmed elevated protein levels of KCNQ2 (Student's  $t$ -test;  $p = 0.0001$ ; Fig. 6d) and KCNQ5 (Student's  $t$ -test;  $p = 0.0005$ ; Fig. 6e), while KCNQ3 protein levels also showed no significant difference (Student's  $t$ -test;  $p = 0.7725$ ; Fig. 6f). Immunofluorescence analysis further revealed that the total percentages of KCNQ2<sup>+</sup> neurons ( $55.83\% \pm 4.06\%$ ) and KCNQ5<sup>+</sup> neurons ( $52.31 \pm 3.78\%$ ) were significantly higher in the BTBR group than in the Con group (KCNQ2<sup>+</sup>  $35.14\% \pm 2.37\%$ , Student  $t$ -test,  $p = 0.0002$ ; Fig. 6g; KCNQ5<sup>+</sup>  $41.76 \pm 2.09\%$  Student  $t$ -test,  $p = 0.0168$ ; Fig. 6h). Size distribution analysis of KCNQ2<sup>+</sup> neuron (Fig. 6k) showed that neurons with a diameter of less than 20  $\mu$ m (Student's  $t$ -test;  $p = 0.035$ ) and those with a diameter between 20 and 30  $\mu$ m (Student's  $t$ -test;  $p = 0.0012$ ) were significantly larger in the BTBR group than in the Con group. Similarly, the size distribution analysis of KCNQ5<sup>+</sup> neurons (Fig. 6l) indicated that neurons with a diameter of less than 20  $\mu$ m (Student's  $t$ -test;  $p = 0.019$ ) and those with a diameter between 20 and 30  $\mu$ m (Student's  $t$ -test;  $p = 0.015$ ) were significantly larger in the BTBR group compared to the Con group.

To further investigate the role of M channels in pain perception, we administered an intrathecal injection of the KCNQ inhibitor XE-991 (30  $\mu$ M) in BTBR mice and observed a significant reduction in baseline mechanical pain threshold at XE-991 1 h (two-way ANOVA;

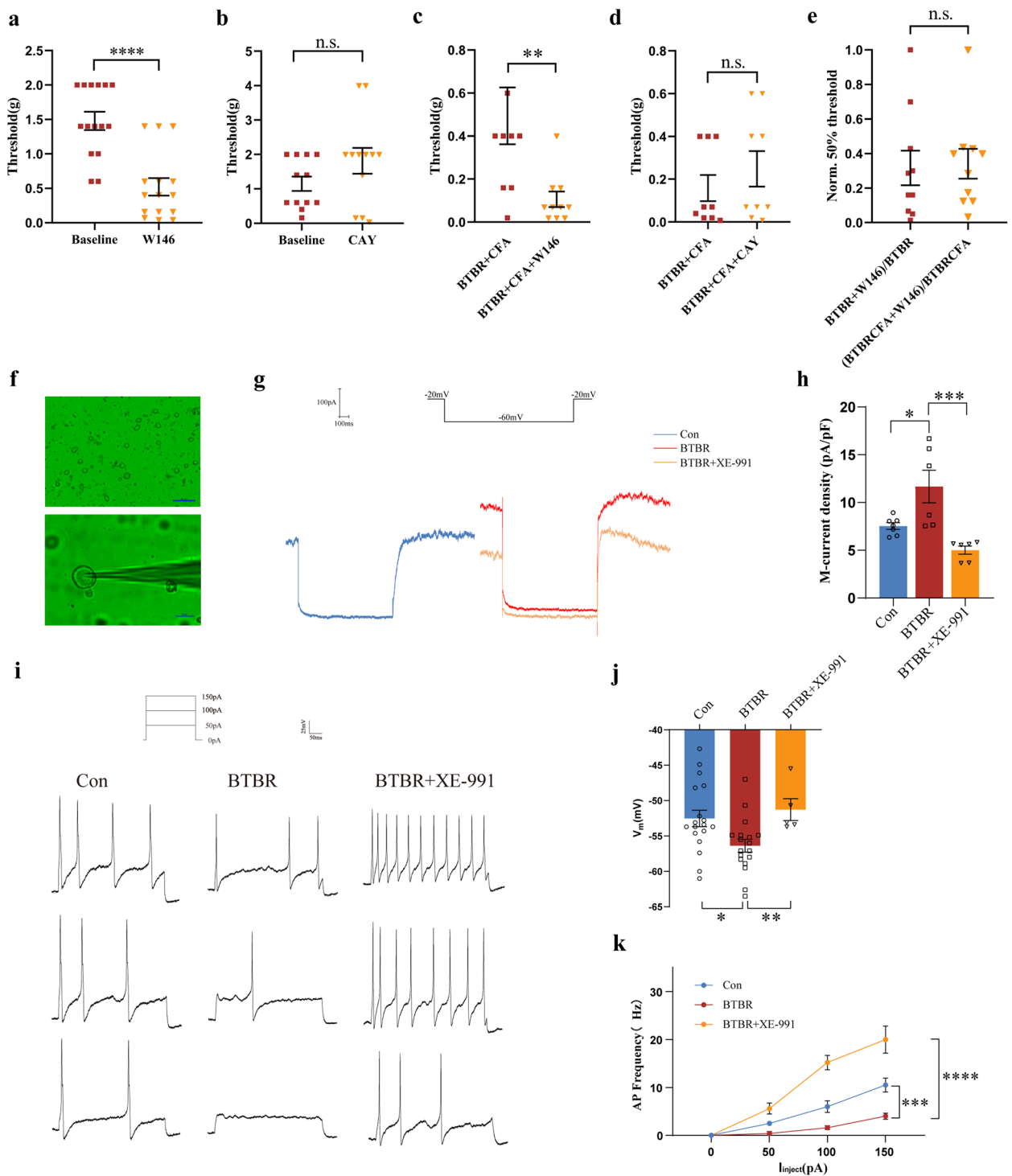


**Fig. 5** S1PR1 inhibitor modulates mechanical pain and quantitative analysis of DRG neurons in BTBR mice. **a** Effect of W146 on baseline mechanical pain in BTBR mice.  $n = 15$  mice per group. **b** Effect of CAY on baseline mechanical pain in BTBR mice.  $n = 12$  mice per group. **c** Effect of W146 on inflammatory pain in BTBR mice.  $n = 8-10$  mice per group. **d** Effect of CAY on inflammatory pain in BTBR mice.  $n = 9$  mice per group. **e** Normalized pain thresholds after W146 intervention in BTBR mice.  $n = 10$  mice per group. **f** Morphological observation of DRG neurons in acutely isolated culture for 24 h. **g** Representative traces of an average current in a single neuron. **h** Quantitative analysis of the KCNQ tail current density.  $n = 6-7$  cells per group. **i** Example traces of a single action potential in DRG neurons of mice, the excitation currents were 50 pA, 100 pA, and 150 pA. **j** RMP in DRG neurons of mice.  $n = 5-18$  cells per group. **k** Action potential firing frequency in DRG neurons of mice.  $n = 5-8$  cells per group. All data are shown in bar and line diagrams, which reflect the arithmetic mean  $\pm$  standard error of the mean. \*  $p < 0.05$ , \*\*  $p < 0.01$ , \*\*\*  $p < 0.001$ , \*\*\*\*  $p < 0.0001$ , n.s. not significantly different

$p=0.0094$ ; Fig. 6m), 1.5 h ( $p=0.033$ ), and 2 h ( $p=0.036$ ) post-injection. These results suggest that PAI in BTBR mice may be attributed to the activation of M channels and the subsequent inhibition of action potentials in DRG neurons.

#### S1PR1 inhibition downregulated M channels, involving MAPK and cAMP/PKA signaling pathways

S1P-S1PR signaling modulates M channel-mediated pain responses by regulating mechanonociceptor excitability [27]. To explore the molecular mechanism underlying S1PR1-mediated PAI in M-channel, we assessed the RNA expression levels of related genes. Our results showed that the upregulation of *KCNQ2* (Student's *t*-test;  $p=0.0249$ ; Fig. 7a) and *KCNQ5* (Student's *t*-test;  $p=0.0155$ ; Fig. 7b) in BTBR mice DRGs was significantly reduced following intrathecal intervention of the S1PR1 inhibitor W146. However, *KCNQ3* expression remained unchanged (Student's *t*-test;  $p=0.9451$ ; Fig. 7c). Western blot analysis further confirmed the reduction in *KCNQ2* (Student's *t*-test;  $p=0.0033$ ; Fig. 7d) and *KCNQ5* (Student's *t*-test;  $p=0.0004$ ; Fig. 7e) expression after W146 intervention. In contrast, *KCNQ3* expression showed no significant difference (Student's *t*-test;  $p=0.2252$ ; Fig. 7f). Immunofluorescence analysis indicated that the total percentages of *KCNQ2*<sup>+</sup> neurons decreased to  $38.00\% \pm 2.09\%$  (Student's *t*-test;  $p=0.0007$ ; Fig. 7g) and *KCNQ5*<sup>+</sup> neurons decreased to  $41.65\% \pm 2.91\%$  (Student's *t*-test;  $p=0.024$ ; Fig. 7h) in BTBR DRG 1 h after W146 intervention. Given the alleviation of PAI behavior following W146 intervention, we conclude that the targeted inhibition of upregulated S1PR1 in the DRGs of BTBR mice could reduce the activation of M channels.

Subsequently, we investigated the signaling pathways involved in nociceptive information, including MAPK, cAMP/PKA, and PKC pathways. Decreased levels of P-ERK/ERK (one-way ANOVA;  $p=0.0396$ ; Fig. 7i), P-P38/P38 (one-way ANOVA;  $p=0.0058$ ; Fig. 7j), and P-PKA/PKA (one-way ANOVA;  $p=0.0177$ ; Fig. 7k) were observed in the DRGs of BTBR mice compared to those of Con mice. Remarkably, these expression levels were significantly upregulated after intrathecal injection of W146: P-ERK/ERK (one-way ANOVA;  $p=0.0073$ ;

Fig. 7i), P-P38/P38 (one-way ANOVA;  $p=0.0056$ ; Fig. 7j), and P-PKA/PKA (one-way ANOVA;  $p=0.0085$ ; Fig. 7k). There were no significant differences in P-PKC/PKC expression between the groups (one-way ANOVA; BTBR vs. Con,  $p=0.4999$ ; BTBR vs. BTBR + W146,  $p=0.7325$ ; Fig. 7l). These findings suggest that aberrant MAPK and cAMP/PKA pathways associated with the development of pain in ASD may be mitigated through S1PR1 inhibition.

#### S1PR1 signaling blocked by SphK inhibitor in DRGs of BTBR mice

We previously elucidated the downstream signaling mechanisms of S1PR1 in ASD PAI. Here, we explore the upstream regulation of increased S1PR1 expression. Our prior study demonstrated elevated S1P levels in the serum of patients with ASD [21]. Despite impaired baseline pain in BTBR mice, accurate quantification of S1P in non-plasma tissues proved challenging. Therefore, we investigated the role of S1P regulation in ASD pain perception by specifically targeting the rate-limiting enzyme, SphK, with its inhibitors SK I II. Intraperitoneal injections of SK I II (50 mg/kg) were administered daily for 14 days to BTBR mice (BTBR + SK I II group) to maintain reduced S1P physiological levels throughout the body. CFA was injected into the left hind paws on day 8. The BTBR + SK I II group exhibited a significant decrease in mechanical pain threshold (Student's *t*-test;  $p=0.0006$ ; Fig. 8a) and thermal pain threshold (Student's *t*-test;  $p=0.0003$ ; Fig. 8b) compared to the BTBR + vehicle (Veh) group. Cointerventions with SK I II and CFA on day 14 (BTBR + CFA + SK I II group) also led to reduced mechanical pain perception compared to the control (BTBR + CFA + Veh) group (Welch's *t*-test;  $p=0.0041$ ; Fig. 8c). Following 14 days of SK I II intervention, RNA-seq analysis of data 2 (Additional file 1: Table S1) was conducted, focusing on significant changes in the DEGs with a screening standard of  $p < 0.05$ . We identified 2898 DEGs in the BTBR and BTBR + SK I II group and found that among all S1PR subtypes, only *S1PR1* was significantly decreased (Fig. 8d and e). Protein expression of S1PR1 expression was downregulated in the DRG of BTBR + SK I II group compared to the BTBR + Veh

(See figure on next page.)

**Fig. 6** Increased expression of *KCNQ2* and *KCNQ5* neurons in DRG of BTBR mice. **a–c** Quantification of *KCNQ2*, *KCNQ5*, and *KCNQ3* mRNA;  $n=8-11$  mice per group. **d–f** Representative western blotting results and quantification of the *KCNQ2*, *KCNQ3*, and *KCNQ5* proteins.  $n=8$  mice per group. **g** and **h** Comparison of the percentage of *KCNQ2*<sup>+</sup> and *KCNQ5*<sup>+</sup> neurons in the BTBR and Con group.  $n=8-14$  mice per group. **i** and **j** Representative images of *KCNQ2* and *KCNQ5* immunofluorescence in mice DRGs. Scale bars = 100  $\mu$ m. **k** and **l** Distribution of *KCNQ2*<sup>+</sup> and *KCNQ5*<sup>+</sup> neurons of different diameters in the Con and BTBR group.  $n=5$  mice per group. **m** XE-991 induced nociceptive behavior in BTBR mice.  $n=6$  mice per group. All data are shown in bar diagrams, which reflect the arithmetic mean  $\pm$  standard error of the mean. \*  $p < 0.05$ , \*\*  $p < 0.01$ , \*\*\*  $p < 0.001$ , \*\*\*\*  $p < 0.0001$ , n.s. not significantly different

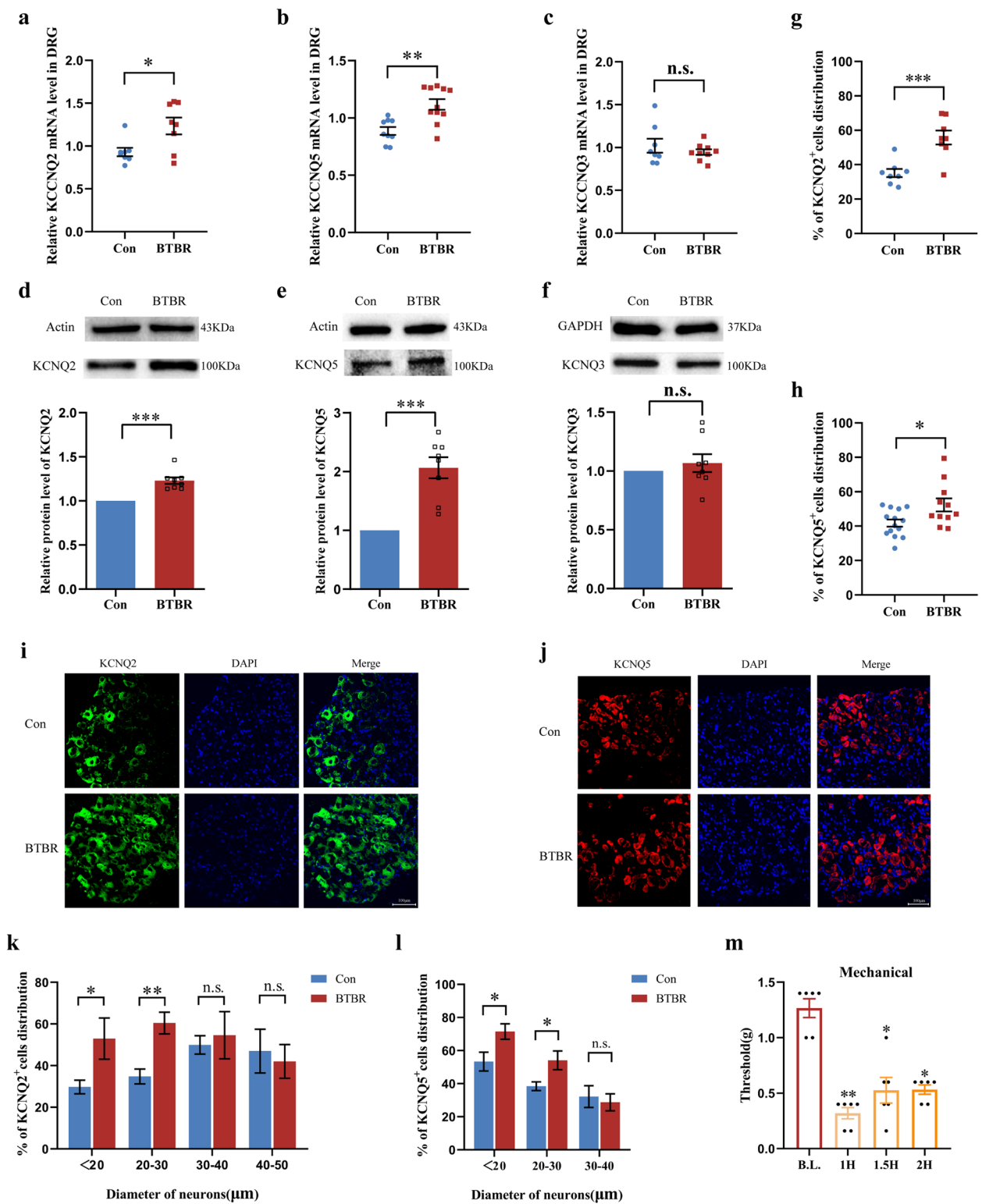


**Fig. 6** (See legend on previous page.)

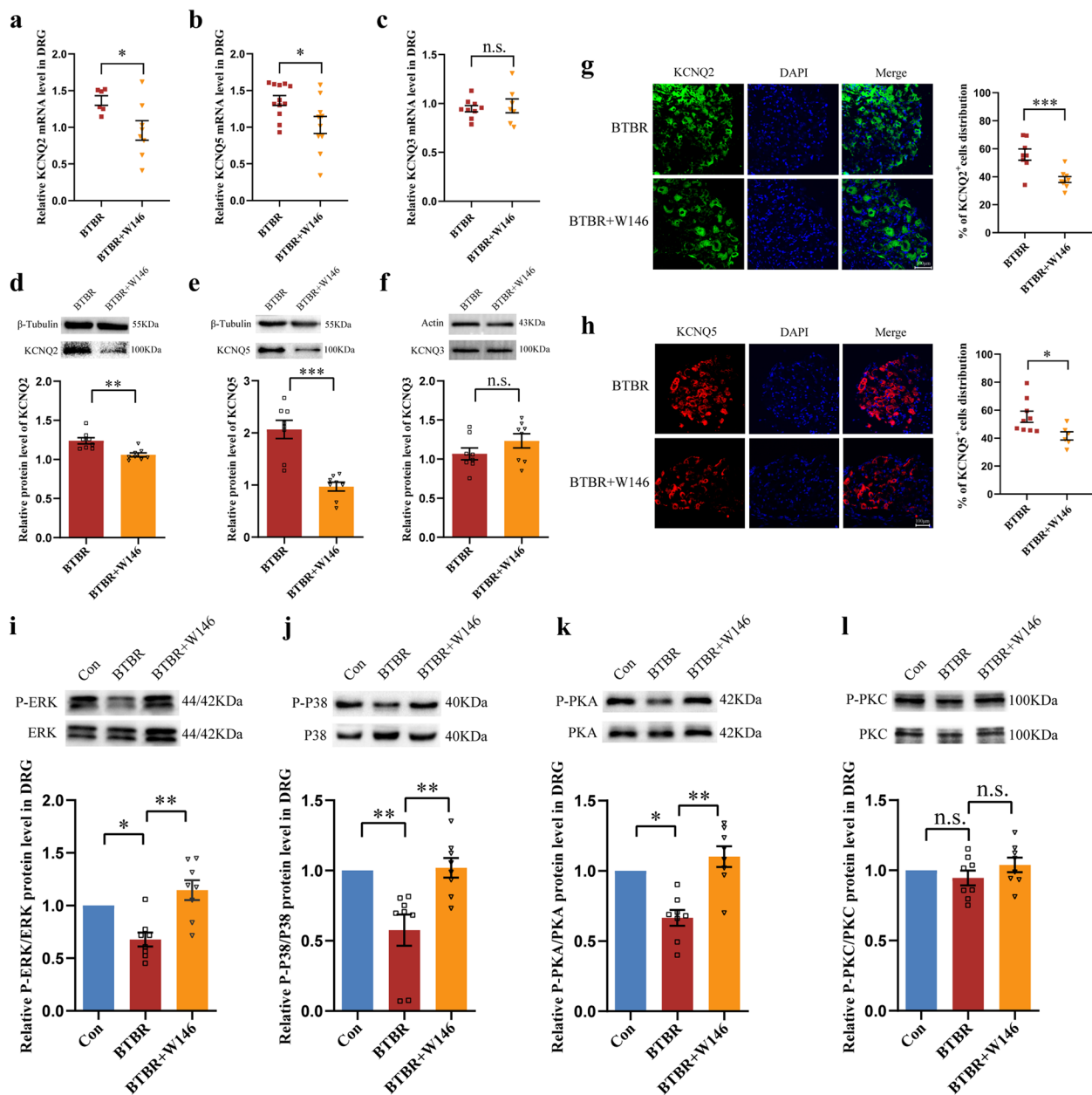


**Fig. 7** M channel and abnormal MAPK cAMP/PKA signaling pathways rescued by inhibition of S1PR1 in mice DRGs. **a–c** Quantification of *KCNQ2*, *KCNQ3*, and *KCNQ5* mRNA levels after the W146 intervention.  $n=6–12$  mice per group. **d–f** Representative western blotting results and quantification of the *KCNQ2*, *KCNQ3*, and *KCNQ5* proteins after W146 intervention.  $n=8$  mice per group. **g** and **h** Representative images of *KCNQ2* and *KCNQ5* immunofluorescence in mice DRGs. Scale bars = 100  $\mu$ m. Comparison of the percentage of *KCNQ2*<sup>+</sup> neurons in the BTBR+W146 and BTBR group;  $n=6–9$  mice per group. **i–l** Representative western blotting results and quantification of P-ERK/ERK, P-P38/P38, P-PKA/PKA, and P-PKC/PKC proteins.  $n=8$  mice per group. All data are shown in bar diagrams, which reflect the arithmetic mean  $\pm$  standard error of the mean. \*  $p < 0.05$ , \*\*  $p < 0.01$ , \*\*\*  $p < 0.001$ , n.s. not significantly different

group (one-way ANOVA;  $p = 0.0013$ ; Fig. 8e). These findings indicate that S1P inhibition ameliorates PAI in BTBR mice by downregulating S1PR1 expression in the DRG.

To further explore the role of S1P in pain modulation, we performed intrathecal injections of exogenous

S1P in Con mice to assess its effects on pain perception. S1P (10  $\mu$ M) produced an analgesic effect, as evidenced by a significant increase in the mechanical pain threshold 1 h post-injection (Fig. 8f; two-way ANOVA;  $p = 0.0009$ ). The pain threshold returned to baseline

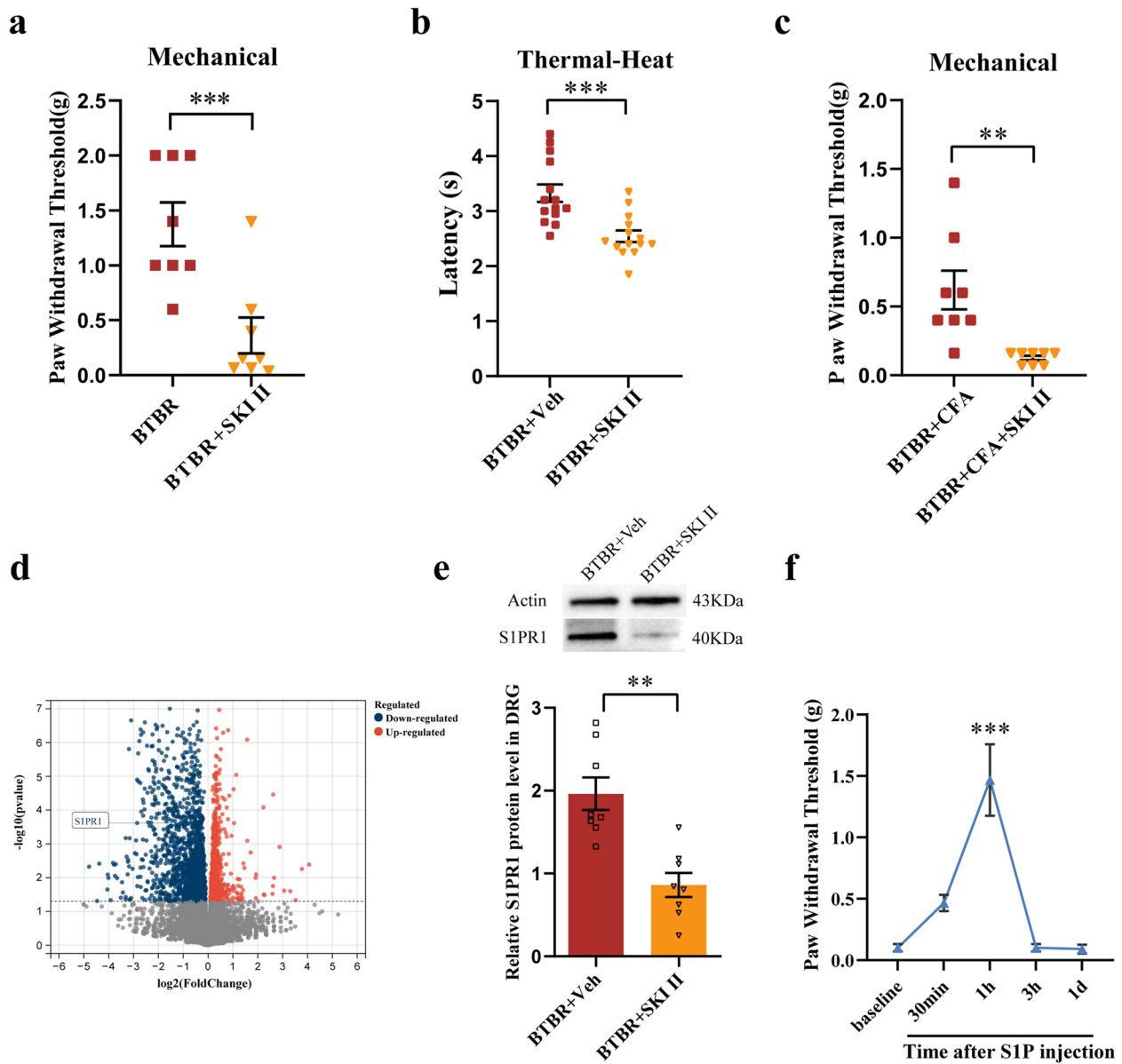


**Fig. 8** S1P/S1PR1 signaling is a critical factor in PAI in BTBR mice. **a** and **b** Mechanical and thermal sensitivity after SKI II intervention in the BTBR group.  $n=8-14$  mice per group. **c** Mechanical sensitivity after SKI II intervention in the BTBR + CFA group.  $n=8$  mice per group. **d** Volcano map showing differentially expressed genes. Red represents upregulated genes, and blue represents downregulated genes. **e** Effect of SKI II on S1PR1 protein expression in BTBR mice, representative western blotting results, and quantification of the S1PR1 protein.  $n=8$  mice per group. **f** S1P induced nociceptive behavior in Con mice.  $n=8$  mice per group. All data are shown as bar diagrams, which reflect the arithmetic mean  $\pm$  standard error of the mean. \*\*  $p < 0.01$ , \*\*\*  $p < 0.001$

levels by day 1 post-intervention ( $p > 0.9999$ ). These data suggest that S1P plays a critical role in mechanical pain and that exogenous S1P induces analgesia in Con mice. The results indicate that the upregulation of S1P/S1PR1 signaling is a key factor in ASD PAI.

### Discussion

ASD is a neurodevelopmental disorder with complex etiology and high heterogeneity [48], and its prevalence is increasing annually, now reaching 1/36 [49]. Abnormal pain perception is a clinical characteristic of patients with

ASD. Many children with ASD exhibit high pain tolerance and infrequent pain expression [50], which substantially contributes to mental disorders [51] and seriously compromise their quality of life as well as their physical and psychological well-being. Previous studies have investigated the involvement of lipid metabolism in ASD pathophysiology [52, 53]. However, the contribution of lipid metabolism regulatory mechanisms to abnormal pain in ASD has not yet been reported.

In this study, we describe a novel mechanism underlying PAI in the peripheral nervous system with ASD. The S1P/S1PR1 signaling could offer a novel therapeutic approach for pain regulation. Here, we report for the first time that the candidate gene *S1PR1*, identified from the GEO database, is closely associated with pain perception in patients with ASD. Our analysis of DRGs in the ASD BTBR mouse model revealed an upregulation of *S1PR1*, further confirming its link with PAI. Inhibiting S1PR1, which is upregulated by SphK, leads to the downregulation of activated M channels in DRGs and improves baseline pain perception in ASD. The MAPK and cAMP/PKA signaling pathways are involved in the regulation of pain perception in ASD via *S1PR1*. Targeting the SphK/S1P/S1PR1 signaling pathway could thus provide a new avenue for clinical interventions aimed at addressing abnormal pain perception in patients with ASD.

Different mouse models exhibit varying responses to sensory abnormalities in ASD, highlighting the complexity of the disorder. Several studies have confirmed that ASD model mice show hyperreactivity to tactile stimulation. For instance, *Gabrb3-ko* and *CDKL 5-ko* mice demonstrate excessive responses to tactile stimuli from the early neonatal stage [54, 55], while *Fmr 1-ko* mice display heightened motor response to repetitive whisker stimuli at postnatal days 14 to 16 [56]. Dysregulation of gene expression in the trigeminal ganglion, which processes input from whiskers, has been observed in *Shank3-ko* and *Cntnap2-ko* mice [57]. Consistent with these findings, we have also demonstrated tactile sensitization in BTBR mice in a separate study. Interestingly, ASD model mice often show reduced sensitivity to pain, a phenomenon supported by genetic studies. For instance, the Shank gene family (*Shank1-3*) has been identified as a risk factor for ASD. *Shank2* knockout mice exhibit analgesia during chronic pain [58], whereas *Shank3* complete knockout mice display impaired heat hyperalgesia during inflammatory and neuropathic pain [19]. Recent studies have shown that *Mecp2<sup>ΔAT-hook1/y</sup>* mutant mice [59], BTBR, and *Fmr1-ko* mice exhibit reduced thermal pain perception in baseline tests, with BTBR mice also showing decreased mechanical allodynia [60]. The *Fmr1-ko* mouse is a widely used model for studying Fragile X syndrome, the most studied monogenic form of ASD [61]. These

findings emphasize the critical role of peripheral somatosensory neurons, leading researchers to focus on this area in ASD research [13]. Tactile hypersensitivity may originate from neural hyperreactivity, whereas insensitivity to pain could be linked to deficiencies in the body's defensive mechanisms. This suggests that touch and pain may be regulated by different neural pathways.

In our study, BTBR mice exhibited significant mechanical and thermal PAI at baseline, as well as CFA-induced inflammatory PAI [60]; however, no difference in neuropathic pain was observed. Notably, BTBR mice demonstrated a faster recovery from mechanical allodynia, with the peak of maximal allodynia occurring on day 5 after injection of CFA. This faster recovery might be attributed to the unique immune profile of BTBR mice, characterized by an enhanced and rapid immune response. BTBR mice show elevated levels of pro-inflammatory cytokines, such as IL-1 $\beta$ , TNF $\alpha$ , and IL-6, along with alterations in immune cell function. This could result from a pre-activated state of their immune cells, enabling a swift response to inflammatory stimuli [62]. Additionally, consistently elevated baseline levels of anti-inflammatory cytokines likely contribute to effectively regulating and control of inflammation. The balance between these pro-inflammatory and anti-inflammatory mediators may be key to the rapid recovery observed. Based on the above evidence, we found that different ASD models showed different pain responses, which aligns with the phenotypic heterogeneity observed in patients with ASD. Overall, we consider BTBR mice to be an ideal ASD model for exploring the pathogenesis of PAI due to their insensitivity to baseline mechanical, thermal, and inflammatory pain.

Addressing the opioid epidemic requires the development of non-narcotic therapies targeting the S1P axis [63], as chronic opioid use often leads to tolerance to analgesics [64]. Lipid S1P signaling is a pivotal regulator and presents a novel target for neuropathic and inflammatory pain [65]. Abnormal lipid accumulation and metabolism are hallmark features of neurodevelopmental and neurodegenerative disorders. Disruptions in lipid metabolism are prevalent in neurological diseases, leading to abnormal lipid accumulation in cells and tissues or interfering with normal metabolic processes. For instance, imbalances in brain ceramide and sphingosine levels are observed in the early stages of neurodegeneration, preceding endomembranous buildup and behavioral changes [66]. Multiple studies have confirmed that abnormal lipid metabolism is frequently observed in patients with ASD and contributes to its pathophysiology [20, 67]. Furthermore, transcriptomic studies in attention deficit hyperactivity disorder have revealed significant changes in lipid metabolism pathways [68], highlighting

the role of lipids in neurodevelopmental disorders. Our prior findings indicated elevated S1P levels in the serum of children with ASD [21]. In BTBR mice, elevated serum and hippocampal S1P levels were reduced by SK I II, leading to improved cognitive function and social ability [22]. Systemic administration of SK I II for 2 weeks reduced S1P production and rescued PAI in BTBR mice, providing evidence that long-term suppression of S1P production can lower the baseline mechanical pain threshold in these mice. Challenges such as matrix effects and lower S1P concentrations complicate the measurement of S1P levels in non-serum tissues. Because S1P expression is similar between serum and peripheral tissues [69], we did not directly assess S1P levels in the DRGs. Instead, we referred to a previous study where we found elevated S1P levels in the serum of BTBR mice, which decreased with SK I II treatment [22]. We speculate that the different phenomena in pain regulation observed between BTBR and Con mice may result from long-term S1P metabolic abnormalities in the peripheral nervous system (PNS) of BTBR mice. Investigating the molecular basis of S1P and its related pathways in the regulation of PAI in ASD holds significant implications.

S1PR1, a downstream receptor of S1P, has emerged as a non-opioid therapeutic target for various pain states [63]. As a G protein-coupled receptor, S1PR1 is involved in multiple intracellular signaling pathways, impacting processes such as ion channel modulation [70, 71]. The involvement of P-Rex1 in S1PR1 signaling has been well-documented, particularly in its crucial roles in neurite maintenance, cell spreading upon S1P stimulation, and neuronal cell-cycle progression [72]. Moreover, S1PR1's differential signaling is integral to nervous system development and plasticity, influencing neuronal differentiation [73], axon growth, and synapse formation [74]. It also plays a pivotal role in guiding the migration of immune cells such as lymphocytes and neural progenitors, essential for immune responses and nervous system development [75]. *S1PR1* is a gene associated with ASD pathology in both humans and mouse models [76]. Systemic administration of an S1PR1 antagonist mitigates cognitive impairment and social deficits associated with elevated central nervous system S1P levels [77, 78], while the S1P/S1PR1 pathway is involved in the development of chronic pain states [63, 79–81]. We demonstrated that S1PR1, regulated by SphK/S1P, is a key downstream signaling pathway involved in PAI. In the spinal cord, increased S1P levels selectively activate S1PR1 in response to neuropathic pain. Inhibition of S1PR1 alleviates and reverses neuropathic pain, and mice with *S1PR1* knockout in the spinal cord are pain-free [82]. S1P and S1PR3 play important roles in acute mechanonociception; ablation of S1PR3 or blockade of S1P in mouse DRG

neurons results in significantly impaired response to mechanical stimuli [27]. Remarkably, in this study, PAI in BTBR mice was attributed to the elevated expression of S1PR1 in the DRG rather than in the spinal cord. We speculate that inhibition of the SphK/S1P/S1PR1 signaling pathway in the DRG may represent a novel therapeutic target for clinical intervention in patients with ASD.

Mutant Kv7 (KCNQ) channels, which alter the generation of action potentials, are potential causative mechanisms of ASD [83–85]. KCNQ2/3 potassium channels are key players in pain signaling and serve as analgesic targets within the peripheral somatosensory system [28]. Intrathecal administration of the M-channel activator retigabine has been shown to alleviate thermal hyperalgesia and mechanical allodynia in Sprague–Dawley rats [86]. Deletion of *KCNQ2/3* potassium channels leads to aberrant neuronal excitability [87], and selective knock-down of Kv7.2 in mouse sensory neurons increases thermal hyperalgesia and mechanical allodynia [88]. Decreased expression of M channels in small-diameter DRG neurons has been reported in mouse models of chronic pain. Our study also found activated M channels in the BTBR mouse DRGs, consistent with the anti-excitatory effect of pain regulation mediated by M-channel openers [89]. Interestingly, overexpression of KCNQ2 channels is involved in hyperalgesia following chronic trigeminal nerve constrictive injury, which contradicts most of the studies mentioned above, possibly due to compensatory changes that limit the hyperexcitability induced by injury [90]. During the regulation of S1P signaling to M channels, endogenous S1P activates S1PR3 signaling and inhibits KCNQ2/3 channels, thereby regulating neuronal excitability [27, 91]. Studies on the regulation of M-currents by repressor element 1-silencing transcription factor in the DRG have led to the identification of a new target for PAI in patients with ASD, and M-channel activation by openers has alleviated chronic hyperalgesia in several pain models [89, 92]. Rest is a neuron-restrictive silencing factor that suppresses M-current density in DRG neurons and is a vital component in the development of mechanical and thermal hyperalgesia [93, 94]. It is hypothesized that the elevated expression of S1P/S1PR1 signaling activates M channels in the DRG of BTBR mice, leading to persistent PAI.

S1P is a well-established extracellular lipid mediator, and its functions are mediated through signaling via specific G protein-coupled receptors (GPCRs) [95]. GPCR signaling pathways also activate Gas- or Gai/o-dependent cAMP/PKA and MAPK pathways [96]. KCNQ2, a voltage-gated potassium channel in the prefrontal cortex, is phosphorylated through the activated PKA/ERK pathway [97], consistent with findings that the open state of KCNQ channels is increased by PKA

phosphorylation, which impairs working memory [98]. Nerve growth factor activates the phosphorylation of MAP kinases (ERK) in neutrophils from healthy individuals, but not in patients with congenital insensitivity to pain with anhidrosis [99]. A significant increase in phosphorylated ERK1/2 contributes to pain hypersensitivity in the DRGs of injured mice [100, 101]. Increased activation of the MAPK pathway (P-ERK and P-P38) has been observed in the hippocampus of neonatal BTBR mice [102, 103], contrasting with our findings in the DRGs of BTBR mice, where the expression of ERK and P38 was reduced. Differential expression of the ERK and P38 pathways is involved in distinct mechanisms in the central nervous system (CNS) and PNS. ERK1/2 are widely expressed in the brain and play crucial roles in regulating neuronal function, neuroinflammation, learning, memory, and synaptic plasticity [104]. In the PNS, ERK1/2 are involved in inflammatory responses, pain signaling, myelin debris clearance, and nerve regeneration [105, 106]. P38 kinase is associated with neuroinflammation in the CNS and impacts neuronal survival, learning, and memory [107, 108]. In the PNS, P38 kinase is important for neuropathic pain and supports axonal regeneration and recovery after nerve injury [109]. The S1PR1 agonist fingolimod alleviates hyperalgesia and reduces P-ERK expression in peripheral neuropathic pain models, whereas the S1PR1 antagonist W146 can reverse these effects [110]. In a mouse model of neuropathic pain, intrathecal delivery of W146 inhibited the MAPK (ERK and P38) pathways in the spinal dorsal horn [111]. Sensory neuronal hyperexcitability is activated by the PKA pathway during the development of various pain-related conditions [112]. Additionally, selective knockdown of PKA by intrathecal small interfering RNA significantly attenuated sustained morphine-mediated thermal and mechanical hyperalgesia in rats [113]. Our study provides novel evidence that inhibiting the overexpression of S1PR1 can rescue baseline PAI in BTBR mice. Furthermore, the decreased ERK, P38, and PKA signaling pathways in the L4-6 DRGs of BTBR mice were reversed.

## Conclusions

S1PR1 may contribute to PAI in the PNS in ASD. The mechanism involves KCNQ/M channels and the MAPK and cAMP/PKA signaling pathways. Targeting S1PR1 in the PNS could offer novel therapeutic strategies for the intervention of pain dysesthesias in individuals with ASD.

## Abbreviations

ASD	Autism spectrum disorder
PAI	Pain insensitivity
S1PR1	Sphingosine-1-phosphate receptor 1
DRG	Dorsal root ganglia
MAPK	Mitogen-activated protein kinase

cAMP/PKA	Cyclic AMP/protein kinase A
Mecp2	Methyl CpG binding protein 2
Gabrb3	Gamma-aminobutyric acid type A receptor subunit beta3
S1P	Sphingosine-1-phosphate
SphK	Sphingosine kinase
CCI	Chronic constriction injury
CFA	Complete Freund's adjuvant
DEGs	Differentially expressed genes
WGCNA	Weighted gene co-expression network analysis
DMEM	Dulbecco's Modified Eagle Medium
ANOVA	Analysis of variance
GPCRs	G protein-coupled receptors
PNS	Peripheral nervous system
CNS	Central nervous system

## Supplementary Information

The online version contains supplementary material available at <https://doi.org/10.1186/s12916-024-03722-3>.

Additional file 1: Tables S1 and S2. Table S1 Characteristics of the datasets. This table outlines the essential features of the four datasets utilized in our study, including the country of origin, experiment type, sample source, sample size with breakdown by control and ASD groups, and the platform used for each dataset. Table S2 Primers used in the study. This table lists the primers employed in the present study, detailing the target gene, forward primer sequence, and reverse primer sequence for each primer set used in our experiments

## Acknowledgements

Not applicable.

## Authors' contributions

Study design: LJW, LLF. Data collection: LLF, QL, YXS, YY, XRZ, XL, YTL, JQC, YQS and AJC. Data analysis: LLF, QL, YTL, JQC, JW. Manuscript preparation: LLF, QL. Manuscript inspection: LJW, LLF, JW. All authors read and approved the final manuscript.

## Funding

This research was supported by funding from the National Natural Science Foundation of China (82073577, 81703251), Heilongjiang Province Natural Science Foundation (grant number LH2022H012), and the Doctor Green Seedlings Ground-Breaking Project of Harbin Medical University (grant number QMPT-1902).

## Data availability

No datasets were generated or analysed during the current study.

## Declarations

### Ethics approval and consent to participate

All animal experiments and procedures were approved by the Ethics Committee of Harbin Medical University (No. HMUIRB20210002). All animal experiments were performed in accordance with a guide to animal ethics.

### Consent for publication

Not applicable.

### Competing interests

The authors declare no competing interests.

### Author details

<sup>1</sup>Department of Children's and Adolescent Health, Public Health College, Harbin Medical University, Harbin 150081, China. <sup>2</sup>School of Nursing, Xuzhou Medical University, Xuzhou 221004, China. <sup>3</sup>Department of Developmental Behavioral Pediatrics, The Sixth Affiliated Hospital of Harbin Medical University, Harbin 150023, China.

Received: 28 June 2024 Accepted: 22 October 2024  
Published online: 04 November 2024

## References

- Orefice LL, Mosko JR, Morency DT, Wells MF, Tasnim A, Mozeika SM, et al. Targeting peripheral somatosensory neurons to improve tactile-related phenotypes in ASD models. *Cell*. 2019;178(4):867–86.e24.
- First MB, Yousif LH, Clarke DE, Wang PS, Gogtay N, Appelbaum PS. DSM-5-TR: overview of what's new and what's changed. *World Psychiatry*. 2022;21(2):218–9.
- Marco EJ, Hinkley LB, Hill SS, Nagarajan SS. Sensory processing in autism: a review of neurophysiologic findings. *Pediatr Res*. 2011;69(5 Pt 2):48R–54R.
- Robertson CE, Baron-Cohen S. Sensory perception in autism. *Nat Rev Neurosci*. 2017;18(11):671–84.
- Balasco L, Provenzano G, Bozzi Y. Sensory abnormalities in autism spectrum disorders: a focus on the tactile domain, from genetic mouse models to the clinic. *Front Psychiatry*. 2020;10:1016.
- Foss-Feig JH, Heacock JL and Cascio CJ. Tactile responsiveness patterns and their association with core features in autism spectrum disorders. *Res Autism Spectr Disord*. 2012;6(1):337–44.
- Allely CS. Pain sensitivity and observer perception of pain in individuals with autistic spectrum disorder. *Sci World J*. 2013;2013(ss03):916178.
- Whitney DG, Shapiro DN. National prevalence of pain among children and adolescents with autism spectrum disorders. *JAMA Pediatr*. 2019;173(12):1203–5.
- Klintwall L, Holm A, Eriksson M, Carlsson LH, Olsson MB, Hedvall A, et al. Sensory abnormalities in autism. A brief report. *Res Dev Disabil*. 2011;32(2):795–800.
- Halayem S, Charfi N, Touati M, Mrabet A, Bouden A. Sensitivity to pain in autistic spectrum disorders: its links with self-aggressivity. *Tunis Med*. 2018;96(8–9):501–4.
- Summers J, Shahrami A, Cali S, D'Mello C, Kako M, Palikucin-Reljin A, et al. Self-injury in autism spectrum disorder and intellectual disability: exploring the role of reactivity to pain and sensory input. *Brain Sci*. 2017;7(11):140.
- Furniss F, Biswas AB. Recent research on aetiology, development and phenomenology of self-injurious behaviour in people with intellectual disabilities: a systematic review and implications for treatment. *J Intellect Disabil Res*. 2012;56(5):453–75.
- Orefice LL. Peripheral somatosensory neuron dysfunction: emerging roles in autism spectrum disorders. *Neuroscience*. 2020;445:120–9.
- Carroll L, Braeutigam S, Dawes JM, Krsnik Z, Kostovic I, Coutinho E, et al. Autism spectrum disorders: multiple routes to, and multiple consequences of, abnormal synaptic function and connectivity. *Neuroscientist*. 2021;27(1):10–29.
- Failla MD, Moana-Filho EJ, Essick GK, Baranek GT, Rogers BP, Cascio CJ. Initially intact neural responses to pain in autism are diminished during sustained pain. *Autism*. 2018;22(6):669–83.
- Chien YL, Wu SW, Chu CP, Hsieh ST, Chao CC, Gau SS. Attenuated contact heat-evoked potentials associated with sensory and social-emotional symptoms in individuals with autism spectrum disorder. *Sci Rep*. 2017;7:36887.
- Vaughan S, McGlone F, Poole H, Moore DJ. A quantitative sensory testing approach to pain in autism spectrum disorders. *J Autism Dev Disord*. 2020;50(5):1607–20.
- Orefice LL, Zimmerman AL, Chirila AM, Sleboda SJ, Head JP, Ginty DD. Peripheral Mechanosensory Neuron Dysfunction Underlies Tactile and Behavioral Deficits in Mouse Models of ASDs. *Cell*. 2016;166(2):299–313.
- Han Q, Kim YH, Wang X, Liu D, Zhang ZJ, Bey AL, et al. SHANK3 deficiency impairs heat hyperalgesia and TRPV1 signaling in primary sensory neurons. *Neuron*. 2016;92(6):1279–93.
- Usui N, Iwata K, Miyachi T, Takagai S, Wakusawa K, Nara T, et al. VLDL-specific increases of fatty acids in autism spectrum disorder correlate with social interaction. *EBioMedicine*. 2020;58:102917.
- Han W, Shuang L, Wang M, Gao J, Wu L, JJoP and Jpn N. Potential serum biomarkers from a metabolomics study of autism. *J Psychiatry Neurosci*. 2016;40(5):140009.
- Li Q, Shi Y, Li X, Yang Y, Zhang X, Xu L, et al. Proteomic-based approach reveals the involvement of apolipoprotein A-I in related phenotypes of autism spectrum disorder in the BTBR mouse model. *Int J Mol Sci*. 2022;23(23):15290.
- Lucaciu A, Brunkhorst R, Pfeilschifter JM, Pfeilschifter W, Subburayalu J. The S1P–S1PR axis in neurological disorders—insights into current and future therapeutic perspectives. *Cells*. 2020;9(6):1515.
- Patti GJ, Yanes O, Shriver LP, Courade JP, Tautenhahn R, Manchester M, et al. Metabolomics implicates altered sphingolipids in chronic pain of neuropathic origin. *Nat Chem Biol*. 2012;8(3):232–4.
- Chen Z, Doyle TM, Luongo L, Largent-Milnes TM and Salvemini DJ. Sphingosine-1-phosphate receptor 1 activation in astrocytes contributes to neuropathic pain. *Proc Natl Acad Sci U S A*. 2019;116(21):10557–62.
- Li C, Li JN, Kays J, Guerrero M, Nicol GD. Sphingosine 1-phosphate enhances the excitability of rat sensory neurons through activation of sphingosine 1-phosphate receptors 1 and/or 3. *J Neuroinflammation*. 2015;12:70.
- Hill RZ, Hoffman BU, Morita T, Campos SM, Lumpkin EA, Brem RB, et al. The signaling lipid sphingosine 1-phosphate regulates mechanical pain. *Elife*. 2018;7:e33285.
- Du X, Gao H, Jaffe D, Zhang H, Gamper N. M-type K(+) channels in peripheral nociceptive pathways. *Br J Pharmacol*. 2018;175(12):2158–72.
- Gamal El-Din TM, Lantini T, Tschumi CW, Juarez B, Quinlan M, Hayano JH, et al. Autism-associated mutations in K(V)7 channels induce gating pore current. *Proc Natl Acad Sci U S A*. 2021;118(45):e2112666118.
- Barkai O, Goldstein RH, Caspi Y, Katz B, Lev S, Binshtok AM. The role of Kv7/M potassium channels in controlling ectopic firing in nociceptors. *Front Mol Neurosci*. 2017;10:181.
- Bennett GJ, Xie YK. A peripheral mononeuropathy in rat that produces disorders of pain sensation like those seen in man. *Pain*. 1988;33(1):87–107.
- Costa B, Comelli F, Bettoni I, Colleoni M, Giagnoni G. The endogenous fatty acid amide, palmitoylethanolamide, has anti-allodynic and anti-hyperalgesic effects in a murine model of neuropathic pain: involvement of CB(1), TRPV1 and PPARgamma receptors and neurotrophic factors. *Pain*. 2008;139(3):541–50.
- Malheiros JM, Lima M, Avanzi RD, Gomes da Silva S, Suchecki D, Guinsburg R, et al. Repetitive noxious neonatal stimuli increases dentate gyrus cell proliferation and hippocampal brain-derived neurotrophic factor levels. *Hippocampus*. 2014;24(4):415–423.
- Bonin RP, Bories C, De Koninck Y. A simplified up-down method (SUDO) for measuring mechanical nociception in rodents using von Frey filaments. *Mol Pain*. 2014;10:26.
- Tegeder I, Del Turco D, Schmidtko A, Sausbier M, Feil R, Hofmann F, et al. Reduced inflammatory hyperalgesia with preservation of acute thermal nociception in mice lacking cGMP-dependent protein kinase I. *Proc Natl Acad Sci U S A*. 2004;101(9):3253–7.
- Kennedy HS, Jones C 3rd, Caplazi P. Comparison of standard laminectomy with an optimized ejection method for the removal of spinal cords from rats and mice. *J Histotechnol*. 2013;36(3):86–91.
- Langfelder P, Horvath S. WGCNA: an R package for weighted correlation network analysis. *BMC Bioinformatics*. 2008;9:559.
- Admoni-Elisha L, Elbaz T, Chopra A, Shapira G, Bedford MT, Fry CJ, et al. TWIST1 methylation by SETD6 selectively antagonizes LINC-PINT expression in glioma. *Nucleic Acids Res*. 2022;50(12):6903–18.
- Cao X, Xu H, Feng W, Su D, Xiao M. Deletion of aquaporin-4 aggravates brain pathology after blocking of the meningeal lymphatic drainage. *Brain Res Bull*. 2018;143:83–96.
- Liu L, Su Y, Yang W, Xiao M, Gao J, Hu G. Disruption of neuronal-glial-vascular units in the hippocampus of ovariectomized mice injected with D-galactose. *Neuroscience*. 2010;169(2):596–608.
- Xia MD, Yu RR, Chen DM. Identification of hub biomarkers and immune-related pathways participating in the progression of antineutrophil cytoplasmic antibody-associated glomerulonephritis. *Front Immunol*. 2022;12: 809325.
- Cai S, Chen Y, Lin S, Ye C, Zheng F, Dong L. Multiple processes may involve in the IgG4-RD pathogenesis: an integrative study via proteomic and transcriptomic analysis. *Front Immunol*. 2020;11:1795.

43. Chapman KB, van Helmond N. Mechanisms of dorsal root ganglion stimulation in pain suppression: time to consider alternative mechanisms of action? *Neuromodulation*. 2018;21:522–3.
44. Raghavendra V, Tanga FY, DeLeo JA. Complete Freund's adjuvant-induced peripheral inflammation evokes glial activation and proinflammatory cytokine expression in the CNS. *Eur J Neurosci*. 2004;20(2):467–73.
45. Mohammad Zakir Hossain, Shumpei Unno, Hiroshi Ando, et al. Neuroglia crosstalk and neuropathic pain: involvement in the modulation of motor activity in the orofacial region. *International Journal of Molecular Sciences*. 2017;18(10):2051.
46. Lin W, Zhao Y, Cheng B, Zhao H, Miao L, Li Q, et al. NMDAR and JNK activation in the spinal trigeminal nucleus caudalis contributes to masseter hyperalgesia induced by stress. *Front Cell Neurosci*. 2019;13:495.
47. Kim YS, Anderson M, Park K, Zheng Q, Agarwal A, Gong C, et al. Coupled activation of primary sensory neurons contributes to chronic pain. *Neuron*. 2016;91(5):1085–96.
48. Baribeau D, Anagnostou E. Novel treatments for autism spectrum disorder based on genomics and systems biology. *Pharmacol Ther*. 2022;230:107939.
49. Maenner MJ, Warren Z, Williams AR, Amoakohene E, Bakian AV, Bilder DA, et al. Prevalence and Characteristics of Autism Spectrum Disorder Among Children Aged 8 Years - Autism and Developmental Disabilities Monitoring Network, 11 Sites, United States, 2020. *MMWR Surveill Summ*. 2023;72(2):1–14.
50. Benich S, Thakur S, Schubart JR, Carr MM. Parental perception of the perioperative experience for children with autism. *AORN J*. 2018;108(1):34–43.
51. Solmi M, Song M, Yon DK, Lee SW, Fombonne E, Kim MS, et al. Incidence, prevalence, and global burden of autism spectrum disorder from 1990 to 2019 across 204 countries. *Mol Psychiatry*. 2022;27(10):4172–80.
52. El-Ansary A, Chirumbolo S, Bhat RS, Dadar M, Ibrahim EM, Björklund G. The role of lipidomics in autism spectrum disorder. *Mol Diagn Ther*. 2020;24(1):31–48.
53. Dorninger F, Forss-Petter S, Wimmer I, Berger J. Plasmalogens, platelet-activating factor and beyond - ether lipids in signaling and neurodegeneration. *Neurobiol Dis*. 2020;145: 105061.
54. Tasnim A, Alkislal I, Hakim R, Turecek J, Abdelaziz A, Orefice LL, et al. The developmental timing of spinal touch processing alterations predicts behavioral changes in genetic mouse models of autism spectrum disorders. *Nat Neurosci*. 2024;27(3):484–96.
55. Pizzo R, Lamarca A, Sassoè-Pognetto M, Giustetto M. Structural bases of atypical whisker responses in a mouse model of CDKL5 deficiency disorder. *Neuroscience*. 2020;445:130–43.
56. He CX, Cantu DA, Mantri SS, Zeiger WA, Goel A, Portera-Cailliau C. Tactile defensiveness and impaired adaptation of neuronal activity in the Fmr1 knock-out mouse model of autism. *J Neurosci*. 2017;37(27):6475–87.
57. Ciancone-Chama AG, Bonaldo V, Biasini E, Bozzi Y, Balasco L. Gene expression profiling in trigeminal ganglia from *Cntnap2*<sup>-/-</sup> and *Shank3b*<sup>-/-</sup> mouse models of autism spectrum disorder. *Neuroscience*. 2023;531:75–85.
58. Ko HG, Oh SB, Zhuo M, Kaang BK. Reduced acute nociception and chronic pain in *Shank2*<sup>-/-</sup> mice. *Mol Pain*. 2016;12:1744806916647056.
59. Xu M, Song P, Huang W, He R, He Y, Zhou X, et al. Disruption of AT-hook 1 domain in MeCP2 protein caused behavioral abnormality in mice. *Biochimica et biophysica acta. Molecular basis of disease*. 2018;1864(2):347–358.
60. Martin LJ, Poulson SJ, Mannan E, Sivaselvachandran S, Cho M, Setak F, et al. Altered nociceptive behavior and emotional contagion of pain in mouse models of autism. *Genes Brain Behav*. 2022;21(1): e12778.
61. Prieto M, Folci A, Poupon G, Schiavi S, Buzzelli V, Pronot M, et al. Missense mutation of *Fmr1* results in impaired AMPAR-mediated plasticity and socio-cognitive deficits in mice. *Nat Commun*. 2021;12(1):1557.
62. Careaga M, Schwartz J, Ashwood P. Inflammatory profiles in the BTBR mouse: how relevant are they to autism spectrum disorders? *Brain Behav Immun*. 2015;43:11–6.
63. Squillace S, Spiegel S, Salvemini D. Targeting the sphingosine-1-phosphate axis for developing non-narcotic pain therapeutics. *Trends Pharmacol Sci*. 2020;41(11):851–67.
64. Corder G, Tawfik VL, Wang D, Sypek EI, Low SA, Dickinson JR, et al. Loss of  $\mu$  opioid receptor signaling in nociceptors, but not microglia, abrogates morphine tolerance without disrupting analgesia. *Nat Med*. 2017;23(2):164–73.
65. Salvemini D, Doyle T, Kress M, Nicol G. Therapeutic targeting of the ceramide-to-sphingosine 1-phosphate pathway in pain. *Trends Pharmacol Sci*. 2013;34(2):110–8.
66. Hebbar S, Khandelwal A, Jayashree R, Hindle SJ, Chiang YN, Yew JY, et al. Lipid metabolic perturbation is an early-onset phenotype in adult spinster mutants: a *Drosophila* model for lysosomal storage disorders. *Mol Biol Cell*. 2017;28(26):3728–40.
67. Yui K, Imataka G, Yoshihara S. Lipid-based molecules on signaling pathways in autism spectrum disorder. *Int J Mol Sci*. 2022;23(17):9803.
68. Lorenzo G, Braun J, Muñoz G, Casarejos MJ, Bazán E, Jimenez-Escrig A. RNA-Seq blood transcriptome profiling in familial attention deficit and hyperactivity disorder (ADHD). *Psychiatry Res*. 2018;270:544–6.
69. Ramos-Perez WD, Fang V, Escalante-Alcalde D, Cammer M, Schwab SR. A map of the distribution of sphingosine 1-phosphate in the spleen. *Nat Immunol*. 2015;16(12):1245–52.
70. Shida D, Takabe K, Kapitonov D, Milstien S, Spiegel S. Targeting SphK1 as a new strategy against cancer. *Curr Drug Targets*. 2008;9(8):662–73.
71. Zahirri D, Burrow P, Großmann C, Müller CE, Klapperstück M, Markwardt F. Sphingosine-1-phosphate induces migration of microglial cells via activation of volume-sensitive anion channels, ATP secretion and activation of purinergic receptors. *Biochim Biophys Acta Mol Cell Res*. 2021;1868(2): 118915.
72. Hampson E, Tsonou E, Baker MJ, Hornigold DC, Hubbard RE, Massey A, et al. P-Rex1 controls sphingosine 1-phosphate receptor signaling, morphology, and cell-cycle progression in neuronal cells. *Cells*. 2021;10(9):2474.
73. Mizugishi K, Yamashita T, Olivera A, Miller GF, Spiegel S, Proia RL. Essential role for sphingosine kinases in neural and vascular development. *Mol Cell Biol*. 2005;25(24):11113–21.
74. Chatzikonstantinou S, Poulidou V, Arnaoutoglou M, Kazis D, Heliopoulos I, Grigoriadis N, et al. Signaling through the S1P–S1PR axis in the gut, the immune and the central nervous system in multiple sclerosis: implication for pathogenesis and treatment. *Cells*. 2021;10(11):3217.
75. Olesch C, Ringel C, Brüne B, Weigert A. Beyond immune cell migration: the emerging role of the sphingosine-1-phosphate receptor S1PR4 as a modulator of innate immune cell activation. *Mediators Inflamm*. 2017;2017:6059203.
76. Duan W, Wang K, Duan Y, Chu X, Ma R, Hu P, et al. Integrated transcriptome analyses revealed key target genes in mouse models of autism. *Autism Res*. 2020;13(3):352–68.
77. Squillace S, Niehoff ML, Doyle TM, Green M, Esposito E, Cuzzocrea S, et al. Sphingosine-1-phosphate receptor 1 activation in the central nervous system drives cisplatin-induced cognitive impairment. *J Clin Investig*. 2022;132(17): e157738.
78. Wu H, Wang X, Gao J, Liang S, Hao Y, Sun C, et al. Fingolimod (FTY720) attenuates social deficits, learning and memory impairments, neuronal loss and neuroinflammation in the rat model of autism. *Life Sci*. 2017;173:43–54.
79. Benarroch EE. What is the role of sphingosine-1-phosphate receptors in pain? *Neurology*. 2021;96(11):525–8.
80. Doyle T, Chen Z, Obeid LM, Salvemini D. Sphingosine-1-phosphate acting via the S1P<sub>1</sub> receptor is a downstream signaling pathway in ceramide-induced hyperalgesia. *Neurosci Lett*. 2011;499(1):4–8.
81. Li J, Wang Q, Gao Y, Ma W, Sun Z, Yu Y, et al. Blocking SphK/S1P/S1PR1 axis signaling pathway alleviates remifentanyl-induced hyperalgesia in rats. *Neurosci Lett*. 2023;801: 137131.
82. Chen Z, Doyle TM, Luongo L, Largent-Milnes TM, Giancotti LA, Kolar G, et al. Sphingosine-1-phosphate receptor 1 activation in astrocytes contributes to neuropathic pain. *Proc Natl Acad Sci U S A*. 2019;116(21):10557–62.
83. Oh H, Lee S, Oh Y, Kim S, Kim YS, Yang Y, et al. Kv7/KCNQ potassium channels in cortical hyperexcitability and juvenile seizure-related death in *Ank2*-mutant mice. *Nat Commun*. 2023;14(1):3547.
84. Lee IC, Yang JJ, Liou YM, Wong SH. KCNQ2 selectivity filter mutations cause Kv7.2 M-current dysfunction and configuration changes manifesting as epileptic encephalopathies and autistic spectrum disorders. *Cells*. 2022;11(5):894.

85. Sands TT, Miceli F, Lesca G, Beck AE, Sadleir LG, Arrington DK, et al. Autism and developmental disability caused by KCNQ3 gain-of-function variants. *Ann Neurol*. 2019;86(2):181–92.
86. Cai J, Fang D, Liu XD, Li S, Ren J, Xing GG. Suppression of KCNQ/M (Kv7) potassium channels in the spinal cord contributes to the sensitization of dorsal horn WDR neurons and pain hypersensitivity in a rat model of bone cancer pain. *Oncol Rep*. 2015;33(3):1540–50.
87. Soh H, Park S, Ryan K, Springer K, Maheshwari A, Tzingounis AV. Deletion of KCNQ2/3 potassium channels from PV+ interneurons leads to homeostatic potentiation of excitatory transmission. *Elife*. 2018;7:e38617.
88. King CH, Lancaster E, Salomon D, Peles E, Scherer SS. Kv7.2 regulates the function of peripheral sensory neurons. *J Comp Neurol*. 2014;522(14):3262–80.
89. Djouhri L, Malki MI, Zeidan A, Nagi K, Smith T. Activation of K(v)7 channels with the anticonvulsant retigabine alleviates neuropathic pain behaviour in the streptozotocin rat model of diabetic neuropathy. *J Drug Target*. 2019;27(10):1118–26.
90. Ling J, Erol F, Gu JG. Role of KCNQ2 channels in orofacial cold sensitivity: KCNQ2 upregulation in trigeminal ganglion neurons after infraorbital nerve chronic constrictive injury. *Neurosci Lett*. 2018;664:84–90.
91. Passmore GM, Selyanko AA, Mistry M, Al-Qatari M, Marsh SJ, Matthews EA, et al. KCNQ/M currents in sensory neurons: significance for pain therapy. *J Neurosci*. 2003;23(18):7227–36.
92. Wang J, Liu Y, Hu F, Yang J, Guo X, Hou X, et al. Activation of neuronal voltage-gated potassium Kv7/KCNQ/M-current by a novel channel opener SCR2682 for alleviation of chronic pain. *J Pharmacol Exp Ther*. 2021;377(1):20–8.
93. Zhang F, Gigout S, Liu Y, Wang Y, Hao H, Buckley NJ, et al. Repressor element 1-silencing transcription factor drives the development of chronic pain states. *Pain*. 2019;160(10):2398–408.
94. Rose K, Ooi L, Dalle C, Robertson B, Wood IC, Gamper N. Transcriptional repression of the M channel subunit Kv7.2 in chronic nerve injury. *Pain*. 2011;152(4):742–54.
95. Kano K, Aoki J, Hla T. Lysophospholipid mediators in health and disease. *Annu Rev Pathol*. 2022;17:459–83.
96. Levesque MV, Hla T. Signal transduction and gene regulation in the endothelium. *Cold Spring Harb Perspect Med*. 2023;13(1):a041153.
97. Tsuboi D, Otsuka T, Shimomura T, Faruk MO, Yamahashi Y, Amano M, et al. Dopamine drives neuronal excitability via KCNQ channel phosphorylation for reward behavior. *Cell Rep*. 2022;40(10):111309.
98. Arnsten AFT, Jin LE, Gamo NJ, Ramos B, Paspalas CD, Morozov YM, et al. Role of KCNQ potassium channels in stress-induced deficit of working memory. *Neurobiology of stress*. 2019;11:100187.
99. Beigelman A, Levy J, Hadad N, Pinsk V, Haim A, Fruchtman Y, et al. Abnormal neutrophil chemotactic activity in children with congenital insensitivity to pain with anhidrosis (CIPA): the role of nerve growth factor. *Clin Immunol*. 2009;130(3):365–72.
100. Liao Y, Ren Y, Luo X, Mirando AJ, Long JT, Leinroth A, et al. Interleukin-6 signaling mediates cartilage degradation and pain in posttraumatic osteoarthritis in a sex-specific manner. *Sci Signal*. 2022;15(744):eabn7082.
101. Yamakita S, Horii Y, Takemura H, Matsuoka Y, Yamashita A, Yamaguchi Y, et al. Synergistic activation of ERK1/2 between A-fiber neurons and glial cells in the DRG contributes to pain hypersensitivity after tissue injury. *Mol Pain*. 2018;14:1744806918767508.
102. Cheng N, Alshammari F, Hughes E, Khanbabaie M, Rho JM. Dendritic overgrowth and elevated ERK signaling during neonatal development in a mouse model of autism. *PLoS ONE*. 2017;12(6):e0179409.
103. Robson MJ, Quinlan MA, Margolis KG, Gajewski-Kurdiel PA, Veenstra-VanderWeele J, Gershon MD, et al. p38 $\alpha$  MAPK signaling drives pharmacologically reversible brain and gastrointestinal phenotypes in the SERT Ala56 mouse. *Proc Natl Acad Sci USA*. 2018;115(43):E10245–54.
104. Sun J, Nan G. The extracellular signal-regulated kinase 1/2 pathway in neurological diseases: a potential therapeutic target (Review). *Int J Mol Med*. 2017;39(6):1338–46.
105. Yi Z, Ouyang S, Zhou C, Xie L, Fang Z, Yuan H, et al. Andrographolide inhibits mechanical and thermal hyperalgesia in a rat model of HIV-induced neuropathic pain. *Front Pharmacol*. 2018;9:593.
106. Hausott B, Klimaschewski L. Promotion of peripheral nerve regeneration by stimulation of the extracellular signal-regulated kinase (ERK) pathway. *Anat Rec (Hoboken)*. 2019;302(8):1261–7.
107. Bachstetter AD, Van Eldik LJ. The p38 MAP kinase family as regulators of proinflammatory cytokine production in degenerative diseases of the CNS. *Aging Dis*. 2010;1(3):199–211.
108. Falcicchia C, Tozzi F, Arancio O, Watterson DM, Origlia N. Involvement of p38 MAPK in synaptic function and dysfunction. *Int J Mol Sci*. 2020;21(16):5624.
109. Huang S, Chen Y, Jia Y, Yang T, Su W, Zhu Z, et al. Delayed inhibition of ERK and p38 attenuates neuropathic pain without affecting motor function recovery after peripheral nerve injury. *Neuropharmacology*. 2022;202:108835.
110. Doolen S, Iannitti T, Donahue RR, Shaw BC, Grachen CM, Taylor BK. Fingolimod reduces neuropathic pain behaviors in a mouse model of multiple sclerosis by a sphingosine-1 phosphate receptor 1-dependent inhibition of central sensitization in the dorsal horn. *Pain*. 2018;159(2):224–38.
111. Janes K, Little JW, Li C, Bryant L, Chen C, Chen Z, et al. The development and maintenance of paclitaxel-induced neuropathic pain require activation of the sphingosine 1-phosphate receptor subtype 1. *J Biol Chem*. 2014;289(30):21082–97.
112. Li ZH, Cui D, Qiu CJ, Song XJ. Cyclic nucleotide signaling in sensory neuron hyperexcitability and chronic pain after nerve injury. *Neurobiol Pain*. 2019;6:100028.
113. Tumati S, Roeske WR, Largent-Milnes TM, Vanderah TW, Varga EV. Intrathecal PKA-selective siRNA treatment blocks sustained morphine-mediated pain sensitization and antinociceptive tolerance in rats. *J Neurosci Methods*. 2011;199(1):62–8.

## Publisher's Note

Springer Nature remains neutral with regard to jurisdictional claims in published maps and institutional affiliations.